Deliverable P2-TB23-4

Active pixels for Star Trackers: Final report

Authors: Stefan Cos, Dirk Uwaerts, Jan Bogaerts, Werner Ogiers

Distribution: 20 hard copies for ESA

Document history record:

issue	Date	description of change
1	24-03-2006	Origination

Table of contents

Applicable documents

Number	Title	Document ID
AD 01	STAR250 detailed specification	APS-FF-DU-03-003
AD 02	STAR1000 detailed specification	APS-FF-DU-03-004
AD 03	STAR250 and STAR1000 Evaluation test report	APS-FF-SC-05-002

1 Introduction

1.1 Scope

This document details the work performed by FillFactory/Cypress and its subcontractors under ESA contract number 17235/03/NL/FM.

After an introduction (section 1), the report discusses the management of the project (section 2), the evaluation of STAR250/STAR1000 (section 3) and the development of HAS and LCMS (section 4). Section 5 contains the conclusions.

1.2 Objectives

The objectives of this project were:
- To perform a complete evaluation of the STAR250 and STAR1000 image sensors and file an application for EPPL entry
- To develop a new generation of image sensors for the following star tracker applications:
  - A Low Cost Low Mass STR (LCMS)
  - A High Accuracy STR (HAS).

The existing STAR250 and STAR1000 sensors are baselined for use in flight sensors, but have to be qualified and placed on the European Preferred Parts List to ensure its suitability for future ESA space missions

In order to fully exploit the APS technology for star tracker applications, a new generation of APS sensors must be designed specifically for this application

The achievement of the objectives will secure the central role for CMOS APS in the attitude sensors of the future and ensure CMOS technology as valid, viable and attractive alternative for CCD's for use in space.

The objectives of this project are very distinct from each other which requires very different tasks and skills

1.3 Company background

FillFactory became operational on January 1st, 2000 and is active in the field of CMOS image sensor development and production. FillFactory is considered to be one of the leading companies in the field of CMOS image sensor development for professional, industrial and scientific applications for the following markets:
- Industrial vision
- Digital Photography
- Medical applications
- Space and Military applications

FillFactory was a spin-off of the Interuniversitary MicroElectronics Center IMEC in Leuven, Belgium. FillFactory became ISO 9000:2000 certification for its quality system by spring 2004.

In August 2004, during the execution of this project, FillFactory was acquired by Cypress Semiconductor and merged into Cypress Semiconductor Corporation Belgium BVBA (CSCB). CSCB currently employs 75 highly qualified people that work on design, characterization, product engineering, test engineering, qualification and testing of image sensors.

CSCB is active on a worldwide scale with major customers in the US, Japan and Europe.

CSCB has already successfully developed a number of CMOS image sensor devices that are currently implemented in a wide range of products. These developments include large area, large resolution and very high frame rate CMOS image sensors, as well as very small area and resolution sensors.

Reference is made to:
- 13.85 M pixel CMOS image sensor in 35 mm format for the Kodak DCS Pro 14n and DCS Pro 14/n (www.kodak.com).
- High-speed image CMOS sensor sensors for the Phantom 4, Phantom 5, Phantom 6, Phantom 7 and Phantom 9 of Vision Research with full synchronous or snapshot shutter (www.visiblesolution.com).
- 4 M pixel sensor for the machine vision camera CSB4000CL for TELI (www.teli.co.jp)
- A high speed image sensor for the HG-100K camera of Redlake (www.redlake.com)
- A high speed, high dynamic range CMOS image sensor with 100 x 100 pixels at 10,000 FPS for the Micamultima camera offered by Brainvision (www.scimedia.com).

FF is recognized as center of expertise for CMOS image sensors for space applications.
The work for ESA was triggered by the development of the so-called Visual Telemetry System (VTS) in cooperation with MMS and DSS/OIP. The VTS camera was developed around the FUGA15 image sensor. The VTS system was successfully flown on the TEAMSAT mission launched by the ARIANE502. On overview of all past and running ESA CMOS image sensor projects is given below:
As IMEC staff:
- SCADES: Visual telemetry system VTS (10208/92/NLFM WO9)
- ASCMSA: IRIS (11970/96/NL/FM)
- VMC Visual Monitoring Camera VMC (XMM Subcontract DSS/OIP-DO)
- ASCOSS: Star tracker (12227/96/NL/SB)
- ARGUS: CMOS imager for remote sensing (12700/98/NL/FM-CCN006)
As FillFactory:
- STARS/ WO3: Image compression Camera (13716/99/NL/FB WO3)
- LCDSS: Low Cost Digital Sun Sensor (14463/00/NL/DS and 14462/NL/DS)
- STARS/OISL: Optical Inter Satellite Link (13716/99/NL/FM-CCN2)
- APS for star trackers (17235/02/NL/FM)
- Radiometric Performance Enhancement Active Pixel Sensor (Subcontractor of IMEC, 16764/03/NL/EC)

In addition to the above ESA projects a number of projects related to CMOS image sensors for space applications was/is carried out on bilateral basis with other space organizations and industries.

Table 1 gives an overview of the FillFactory space related activities
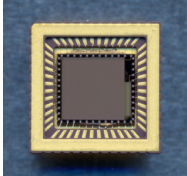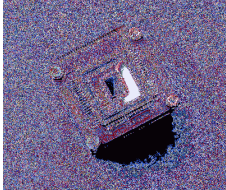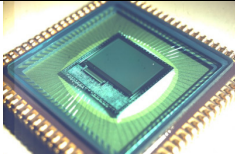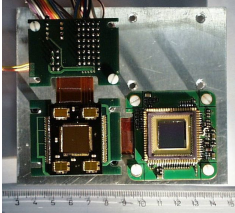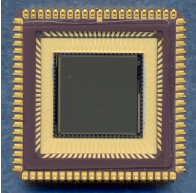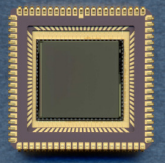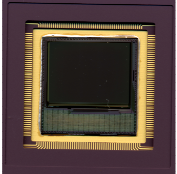
FUGA15		
IRIS-1		
IRIS-2		
ASCOSS		
OISL (STAR250)		
LCDSS (STAR1000)		
IRIS-3		

Table 1. Overview of Space related activities

1.4 Evaluation of STAR250/STAR1000

The existing STAR250 and STAR1000 have been developed in the past under ESA contracts, respectively as OISL and LCDSS. The high tolerance to ionizing radiation makes these sensors very attractive for use in AOCS (Attitude and Orbit Control Systems). The sensors have been characterized in the framework of the respective ESA contracts, but a complete evaluation is necessary in order to make these sensors valid candidates for space missions.

The European Space industry is developing new equipment based on APS, but currently no APS sensors are listed on the EPPL. Therefore evaluation and EPPL entry is necessary to secure the ongoing developments.

1.4.1 STAR250

The base line of the STAR250 sensor design consists of an imager with a 512 by 512 array of active pixels at 25 µm pitch. The detector contains on-chip correction for Fixed Pattern Noise (FPN) in the column amplifiers, a programmable gain output amplifier and a 10-bit Analog to Digital Converter (ADC). Through additional preset registers the start position of a window can be programmed to enable fast read out of only part of the detector array.
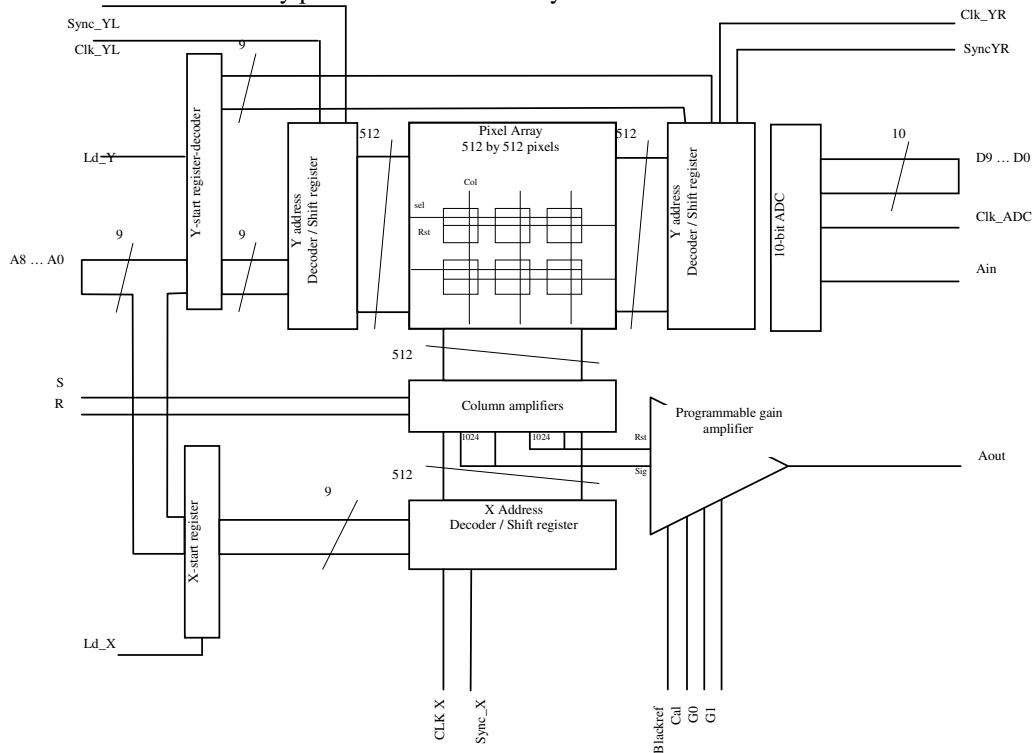
Figure 1.   STAR250 schematic
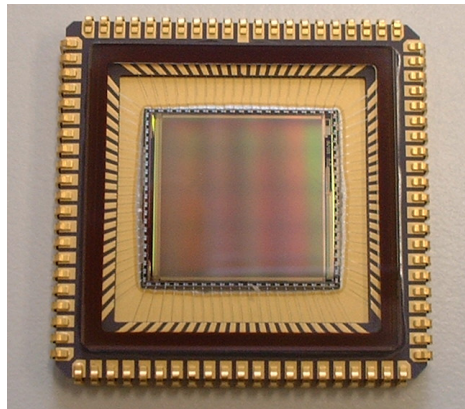
Figure 2.   STAR250 image sensor

1.4.2 STAR1000

The STAR1000 is a CMOS image sensor with 1024 by 1024 pixels on a 15-μm pitch. It features on-chip Fixed Pattern Noise (FPN) correction, a programmable gain amplifier and a 10-bit Analog to Digital Converter (ADC).

All circuits are designed using the radiation tolerant design rules for CMOS image sensors to allow a high tolerance against total dose effects.

Registers that can be directly accessed by the external controller contain the X- and Y-addresses of the pixels to be read. This architecture provides flexible operation and allows different operation modes like (multiple) windowing, sub sampling, etc.

Figure 3.   STAR 1000 schematic

Figure 4.   STAR1000 image sensor

1.4.3 Assembly configuration

Both sensors are assembled in a JLCC 84 pins ceramic package and covered with a glass lid. For the space qualified version it was chosen to use a BK7 glass lid and fill the cavity with dry nitrogen. Table 2 lists the differences between the standard product and the space product.

	Standard product	Space product	Driver
Window	Quartz	BK7G18	Radiation hardness and thermal expansion
Window	Delo	Epotek	Hermeticity and low outgassing
Cavity	Air-filled	N_2-filled	Moisture level

Table 2. Difference between standard product and space product

1.4.4 Evaluation program

It was chosen to do a complete evaluation conform to ESCC 2269000 and apply for EPPL entry. The full qualification, conform to ESCC 9020, and QPL entry is outside the scope of this project but it stays open as an option. An evaluation program is similar to a qualification, but the devices are overstressed to detect the different failure modes. For example mechanical vibration is performed with 50 cycles in stead of 5 cycles.

In the past, both STAR250 and STAR1000 have been characterized and radiation testing was performed to demonstrate radiation tolerance.

The evaluation program is conforming to ESCC 2269000 and consists of:

- Initial measurements
- A control group
- Temperature step stress test
- Radiation tests, including total dose, proton and SEU
- Construction analysis
- Package tests (thermal, mechanical, environmental)
- Electrical tests
- Endurance test

1.5 Development of HAS/LCMS

In recent years CMOS technology has proven itself as a real alternative for CCD technology for the fabrication of image sensor devices. Although CMOS lags behind CCD technology in terms of dark current and read noise performance, state-of-the-art devices as the STAR250 and STAR1000 have demonstrated an acceptable and practical electro-optical performance combined with an unrivaled radiation tolerance. The facts that:

- CCD's superior initial dark current rapidly degrades to CMOS levels of dark current when irradiated
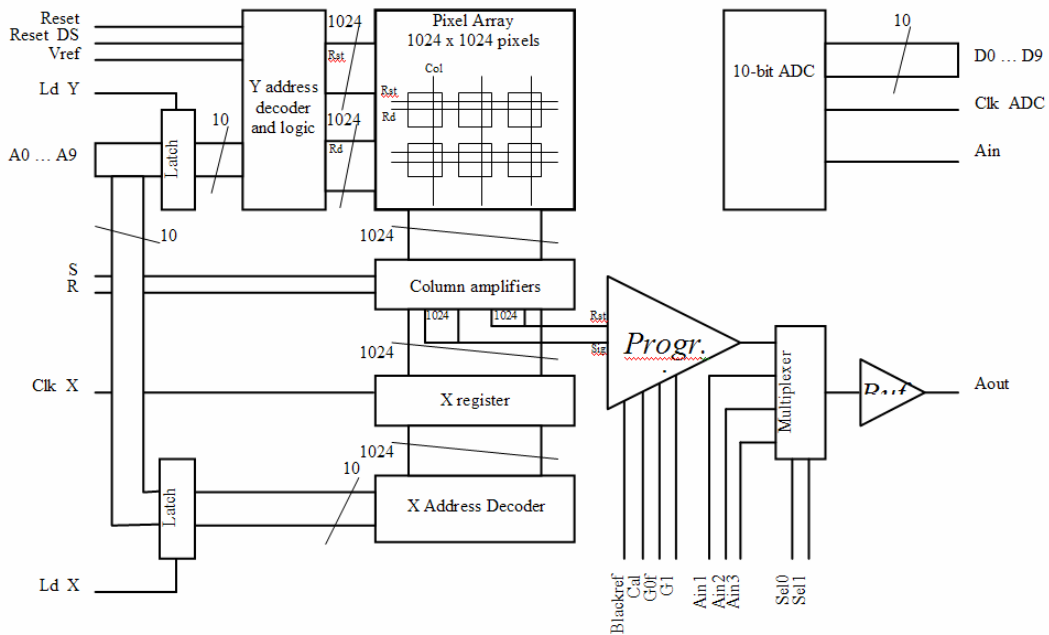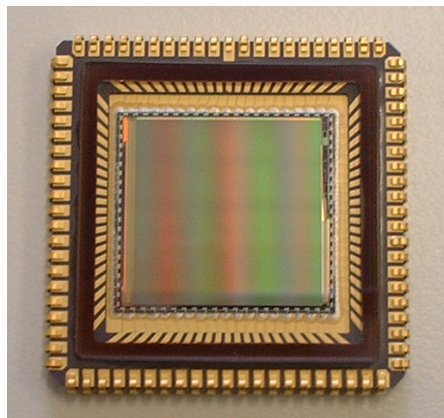- CMOS offers substantially simpler system integration
- CMOS is not yet at the end of its technological development;

promises that CMOS APS will be the technology of preference for future star tracker-like applications. Since the development of STAR250 and STAR1000 a lot of know how was generated that could be used in a new generation of image sensors designed specifically for star tracker applications.

The HAS is a CMOS image sensor for a high accuracy star tracker with substantially improved electro-optical performance.

The LCMS is a technology demonstrator for a future low cost, low mass STR characterized by very high levels of integration and therefore demanded a high level of on-chip functionality to reduce the STR component count.

Initially the HAS and LCMS were scheduled to be developed in parallel. However during the execution of the project it was chosen to do a sequential development, with the LCMS being a derivate (less pixels) from the HAS and on-board digital functionality. This approach reduces the development risk of the analog part of the LCMS, since the HAS serves as a demonstrator for the LCMS analog part.

2 Project management

2.1 Structure

The project consists of 2 main and distinctly different tasks each having 2 phases. The following table gives an overview of the split in tasks and phases:

Task	Phase 1	Phase 2
STAR250/STAR1000 evaluation	Evaluation testing	Re-testing and EPPL application
HAS/LCMS development	HAS design, production and testing LCMS design	LCMS production and testing

This combination of 2 tasks and 2 phases has lead to complexities in the management of the project resulting in some issues with the scheduling (see further).
Figure 5 shows an overview of the project structure/organization.

Figure 5. Project structure

2.2 Schedule

The Request for Quotation was issued 4 September 2002. The project was kicked off 10 April 2003
With an initial duration of 19 months, the project was originally scheduled to end in October 2004. It
ended December 2005.

The following tables give an overview of the scheduling of the main events:

STAR evaluation event	Original date	Actual date
TRR	3 Sept 2003	1 Dec 2004
TRB	2 Jan 2004	19 May 2005
End	19 Oct 2004	10 March 2006

HAS/LCMS event	Original date	Actual date
HAS CDR	28 Jan 2004	7 Nov 2003
HAS TRR	25 May 2004	24 March 2004
HAS TRB	19 Oct 2004	29 June 2004
LCMS CDR	28 Jan 2004	25 Oct 2004
LCMS TRR	25 May 2004	17 March 2005
LCMS TRB	19 Oct 2004	9 Sept 2005

The main reasons for the delay in the STAR evaluation are:
- The assembly of the devices for the evaluation program had to be done over because a wrong curing temperature resulted in major gross and fine leak problems.
- The lack of knowledge on image sensors at the test house resulted in a number of tests that had to be redone
- The endurance test on STAR1000 failed after 168h caused by an incorrect voltage level of the applied clock. The test had to be re-started with spare devices.
- Some unexpected results (moisture level, annealing) caused a number of investigations and re-tests
- Some test methods were not suitable for an image sensor in general or the STAR250/STAR1000 in particular, resulting in additional investigations

The main reason for the delay in the HAS/LCMS development is:
- The parallel development of HAS and LCMS was changed during the project into a sequential development. With the LCMS being a derivate (less pixels) from the HAS with additional on-board digital functionality, this approach reduces the development risk of the analog part of the LCMS, since the HAS serves as a demonstrator for the LCMS analog part.

Figure 6 shows the schedule of the project. The Grey bars are the original schedule; the blue bars are the final schedule.

ID	Task Name
1	M1 Kick-off
2	Project management
3	**Phase 1**
4	STAR evaluation
5	detailed spec
6	suppliers
7	PID
8	PID and Specification Review
9	test preparation
10	TRR
11	evlauation test
12	Test review meeting
13	**test structures and HAS PDR**
23	**HAS/LCMS**
24	HAS design
25	LCMS digital design
26	CDR HAS + IDR LCMS
27	HAS design completion
28	HAS manufacturing
29	M5 TRR HAS
30	HAS testing
31	LCMS prototyping
32	LCMS analogue design
33	LCMS PDR
34	HAS report
35	TRB HAS
36	LCMS design integration
37	LCMS CDR
38	**Phase 2**
39	STAR evaluation
40	evaluation re-testing
41	EPPL application
42	**LCMS**
43	LCMS/DCC tape-out
44	LCMS manufacturing
45	M5 TRR LCMS
46	LCMS testing
47	LCMS report
48	TRB LCMS
49	Final Presentation
50	Industrial support

Figure 6.   Schedule

2.3 CCN

This section gives an overview of the Contract Change Notices that were raised during the project.

2.3.1 CCN1/CCN2

CCN1 and CCN2 were initiated to formalize the sequential development of HAS and LCMS (in stead of the initially planned parallel development). This resulted in a changed planning and a changed payment plan but did not affect the scope of the work.

2.3.2 CCN3

CCN3 was initiated to re-perform a partial re-characterization of the HAS image sensor with a customer specific timing diagram. This work was needed to investigate the extent to which the applied timing affected the performance characteristics of HAS and was in support of the Bepi Colombo project. The work was performed in November/December 2005.

2.4 Lessons learnt

The following lessons were learnt for the management aspects of the project:
- A more detailed verification of alternatives for the project structure and event sequence prevents the project from being re-organized during execution.
- The proposed timing did not contain sufficient time for verifying new things (assembly configuration, test methods, …)

3 Evaluation of STAR250/STAR1000

The objective this work was to perform a complete evaluation of the existing STAR250 and STAR1000 image sensors and to file an application for entry in the European Preferred Parts List (EPPL). For this purpose the work was approached in two phases: Firstly, the main phase of the project comprised the thorough evaluation testing of both image sensors according to established ESA standards (ECC 2269000). In the second phase, some re-testing was performed, based upon what was learned in the first phase and an application for EPPL-entry was filed.

3.1 Phase 1: Detailed evaluation of STAR250 and STAR1000

After design, the devices were produced in prototype quantities and went through a standard electro-optical evaluation at FillFactory to confirm the predicted specifications. The radiation tolerance of the STAR250 device was thoroughly evaluated as part of the Ph. D. thesis of Dr. Jan Bogaerts and the STAR1000 sensor was briefly tested for total dose radiation tolerance in the course of the LCDSS project. Furthermore, the sensors went through some environmental tests as part of the evaluation of the instrument they were build in: STAR 250 in the sun sensor by TNO-TPD and Sodern, STAR1000 in the LCDSS sun sensor by Galileo and the VNI (STAR65) sensor as part of the Atmospheric Chemistry Experiment (ACE) of ABB Bomen for the Canadian Space Agency CSA.

These limited evaluations and tests confirmed that the sensors complied with the design specifications and that they have a good potential to be used in flight hardware. However, in order to become a real candidate for application in commercial and scientific space missions the components must be fully qualified, implying lot acceptance testing and screening.

In order to qualify a component, its procurement process must be fully defined and under control, the component must be fully characterized and the acceptance limits must be fixed. This leads to the following requirements and tasks:

- To review and update the existing ISO 9001 procedures for procurement, inspection and testing.

- To compile a Process Identification Document (PID) that describes in detail the components and the way they are fabricated and procured.

- To conduct an evaluation campaign that will stress the parts until they break in order to reveal the operational limits.

Although a number of procedures for procurement, inspection, testing already existed, FillFactory did not have an ISO9001 qualification at the time the project started. At the beginning of the project these procedures were updated and missing procedures were added and the ISO 9001 qualification was obtained on April 22nd, 2004.

The definition of the PID required more precise specification of all supplied parts: package, glass lid and the manufacturing process required closer attention. The beginning of the project was also a good opportunity to change some parts and to adapt the work flow to ensure better suitability for space use. As such, the glass lid, the gluing material, the alignment process and the final assembly procedure were changed. At the packaging house a special assembly procedure for space products was set up and put to work.

- Glass lid
  For the glass lid specification a survey was done amongst the most important clients of the image sensor to find out their requirements. The final glass lid specifications: material and anti-reflective coating are a super-set of the gathered requirements.

- Gluing material
  Both the die attach material as the glass lid epoxy were investigated more closely from outgassing and strength point of view. Suitable materials were identified in NASA specifications on outgassing and later experimentally verified at the packaging house.

- Die alignment
  Special attention was paid to die alignment and verification. A verification step was added in the packaging work flow to re-measure automatically the die alignment after placement.

- Final assembly:
  In order to maintain a low dew-point the final assembly of the glass lid on the package was moved to a dry nitrogen atmosphere.

3.2 Phase 2:Re-test and EPPL application

After investigation of the results of the first phase a number of tests were repeated:
The following tests were repeated:
- Thermal characterization
- Mechanical shock and vibration
- RGA

The assembly process was improved during phase 2:
- Dimension check
- Die bond coverage
- Wire bond tails
- Additional bake-out to reduce moisture level inside

The EPPL application was prepared.

Evaluation test plan

The evaluation test plan for the STAR250 and STAR1000 image sensors was based upon ESA basic specification ESCC 2269000. Provisions were made to join the STAR250 and STAR1000 evaluation programme and where possible to avoid similar tests. Figure 7 shows an overview of the entire evaluation plan. In total 67 STAR250 and 76 STAR1000 devices were submitted to the tests.

After procurement (P4) of sufficient devices, the complete batch was subjected to inspection (P5) resulting in a list of devices that were to be used for the evaluation program. Special attention was paid to maintain a control group of 10 devices of each kind that did not undergo any stress. During all subsequent measurements before and after stress, burn-in or radiation these devices were measured in the same measurement session to prove the proper operation of the test infrastructure.

During the initial measurements (P6) all devices were characterized at room temperature and at the extreme operating temperatures: -40 °C and +85 °C. Next two subgroups were formed to perform the destructive tests and the endurance tests. Apart from these groups the control group was selected and 5 devices of each were kept apart as reserve.

The destructive tests (Group 2) consisted of the following parts:

- A step-stress test to determine the temperature at which to conduct the endurance test.

- A radiation test containing total dose, proton and heavy ion irradiation. It was decided to re-use the already available proton irradiation test results for STAR250. The total dose radiation tests for STAR250 were repeated because they were only executed on a limited number of samples before. For Heavy ion irradiation no results were available.

- Construction analysis by ESTEC to verify the design of the product.

- Package tests to verify the assembly configuration (combination of package, die and glass lid)

- Electrical tests consisting of ESD tests and parametric tests in function of temperature and supply voltage.
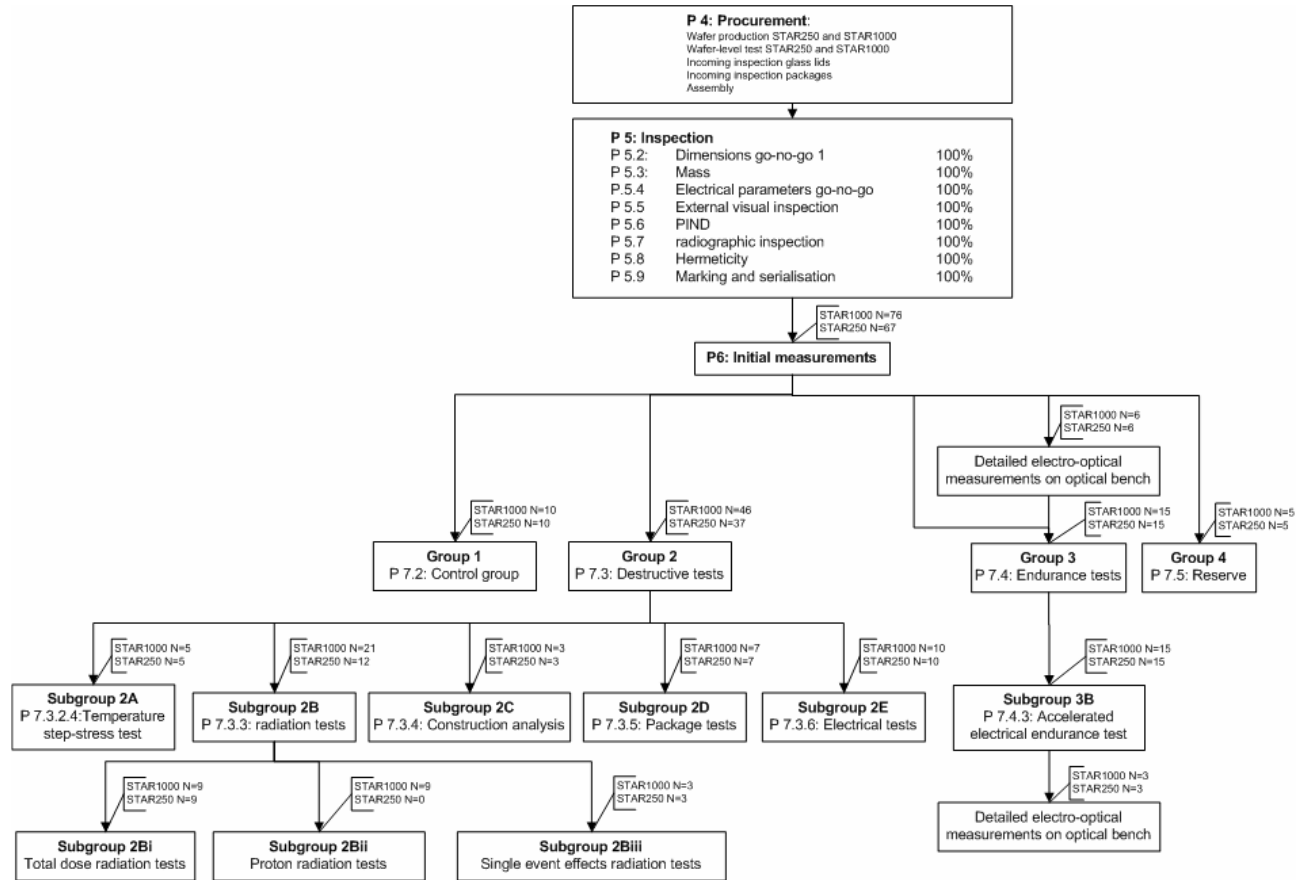
Figure 7.   Evaluation program overview

3.3 Evaluation test results

3.3.1 Initial inspections and tests (P5)

All initial inspections and tests are 100% testing (68 STAR250 and 94 STAR1000)

3.3.1.1 *Dimensions check*

Outer dimensions as well as die positioning have been measured and specs have been defined. The following has been measured:

- Total thickness (glass lid + epoxy + package)
- Die positioning in X and Y
- Tilt (Z positioning)

3.3.1.1.1 Total thickness

Figure 8 shows a cross section of STAR250-STAR1000. The total thickness (glass lid + epoxy + ceramic) was measured:

- The Drawing Spec is: 2.798 mm (+0.272; -0.262)
- The Average $\pm 3\sigma$ is: 2.801 mm ± 0.033

The specification in the detailed specs [AD01 and AD02] is set to 2.8 $\pm$ 0.1 mm
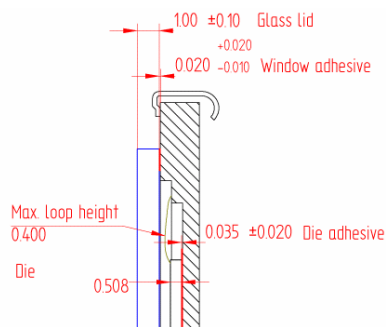
Figure 8.   cross section

3.3.1.1.2 X-Y positioning

Table 3 gives an overview of the X-Y positioning specs and results for STAR250 and STAR1000. X-Y positioning consists of shift in X, shift in Y and parallelism. Figure 9 shows the die positioning drawing for STAR250, Figure 10 shows the die positioning drawing for STAR1000.

The Y-shift results are marginally out of the drawing specification. Therefore the spec in AD01 and AD02 is set wider. However the positioning will be corrected with the assembly house for the future assembly jobs.

	Drawing	**Result ± 3σ**	**Spec [AD01, AD02]**
STAR250 – X shift	0 ± 0.050 mm	0.020 ± 0.020 mm	0 ± 0.050 mm
STAR250 – Y shift	0.068 ± 0.050 mm	0.122 ± 0.022 mm	0.068 ± 0.100 mm
STAR250 – parallelism	± 0.050 mm	± 0.025 mm	± 0.050 mm
STAR1000 – X shift	0.052 ± 0.050 mm	0.034 ± 0.035 mm	0.052 ± 0.050 mm
STAR1000 – Y shift	0.200 ± 0.050 mm	0.240 ± 0.017 mm	0.200 ± 0.100 mm
STAR1000 – parallelism	± 0.050 mm	± 0.029 mm	± 0.050 mm

Table 3.   X-Y positioning results
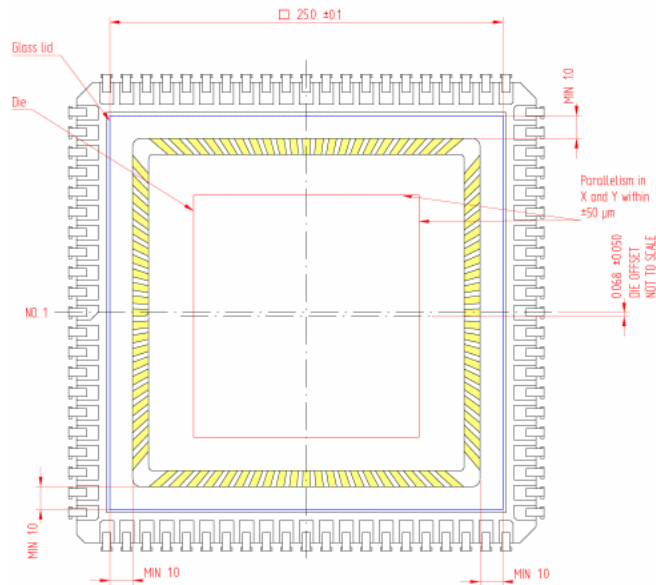
Figure 9.   Die positioning STAR250
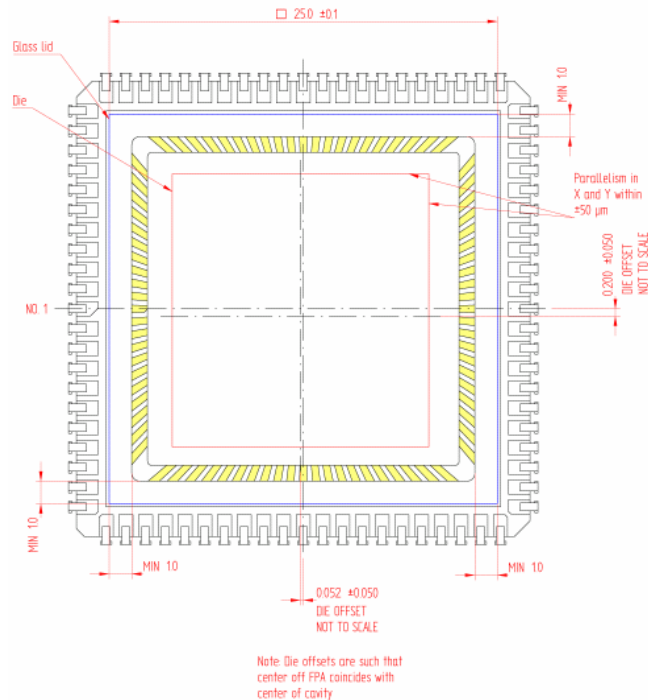
Figure 10.   Die positioning STAR1000

3.3.1.1.3   Tilt

Tilt (or Z-positioning) is the difference between maximum and minimum distance between the 4 corners of the die and the bottom of the cavity. This was not specified before. The results are between 9 and 53 µm. The spec in AD01 and AD02 is set to max 0.100 mm.

3.3.1.2 Weight

The devices have been weighted and a specification was defined:

Specification	min	typical	max
STAR250	6.2g	6.45g	6.7g
STAR1000	6.3g	6.55g	6.8g

3.3.1.3 Electrical measurements

This electrical test was done to exclude non-functioning devices or devices with gross failures due to assembly yield. Some weaknesses were reported and the results have been used for the device distribution over the different tests:

- A STAR250 with a high number of PRNU defects was used for constructional analysis
- A STAR1000 with a significantly lower stand-by current was kept as reserve and is later on used for the 2nd series of endurance tests
- A STAR1000 with a significantly higher ADC DNL and INL was used in the 1st endurance test.

3.3.1.4 External visual inspection

The external visual inspection covers all external visual issues and an internal visual inspection for particles. Specifically the following is inspected:

- Pins (not bent)
- Glass lid (scratches, stains, damage, position, …)
- Epoxy (width, no openings, …)
- Ceramic (cracks, …)
- Outside contamination (glue, …)
- Inside contamination (particles

The following issues have been reported:

- Bent pins (56 STAR250, 55 STAR1000)
- Particles (4 STAR1000)
- Marks on glass (7 STAR250, 4 STAR1000)
- Glue on pins (3 STAR250, 2 STAR1000)
- Loose piece of bonding wire inside (1 STAR1000)

The bent pins are caused by the transport container. A new type of container was developed in phase 2 and is now used as standard tray for JLCC84 devices.

The marks on glass, particles and glue on pins are considered to be assembly yield. These are failures for flight devices but were accepted for the evaluation program, because the failures will not influence the results of the evaluation. For FM devices, these issues are covered by the visual inspection.
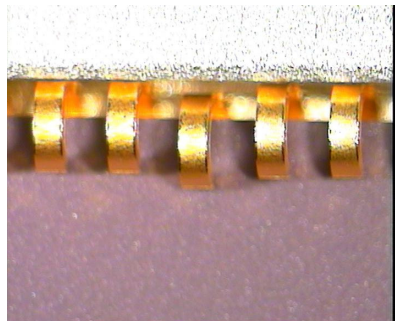

Figure 11.   Photo of bent pins

3.3.1.5 PIND

1 failure reported due to a loose piece of bonding wire in the cavity. This failure was also captured by the internal visual inspection performed before the evaluation program. It was concluded that the PIND test itself does not have the required sensitivity to detect of particles of 20 µm (maximum allowed size). However the combination of a visual inspection (before and after) and a PIND tests allows distinguishing between mobile and fixed particles.

3.3.1.6 Radiographic inspection

Die bonding coverage of STAR1000 was found to be insufficient with voids in the die mount. This is a typical problem for big dies. The die bonding process was improved at the assembly house and 100% XRAY inspection will be done on FM devices. Die pull tests by the assembly house showed results between 180N and 290N. This was documented in NCR019. Figure 12 shows an X-ray photograph of a STAR1000 (epoxy is dark and voids are light).
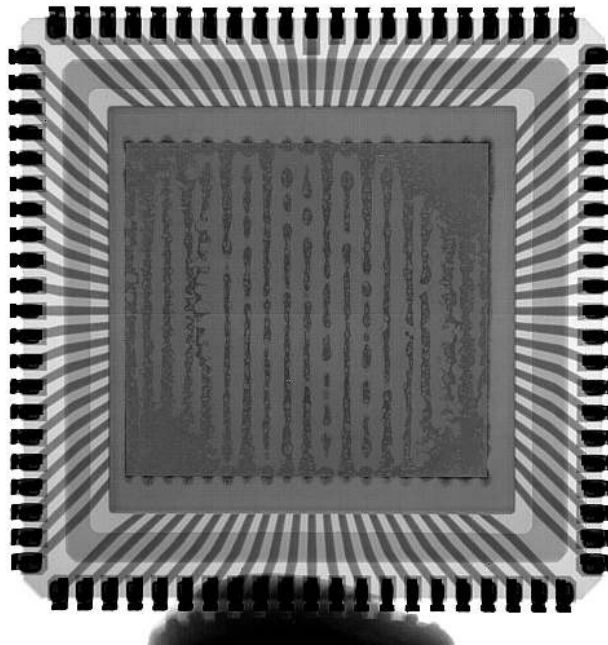
Figure 12.   X-ray photograph of STAR1000

3.3.1.7 Hermeticity

The hermeticity test consists of a gross leak test and a fine leak test.

3.3.1.7.1 Gross leak

A number of gross leak failures were reported. Because the impact of the perfluorocarbon of dye-penetrant test on image sensors is not known, an alcohol bubble test was done. This is not a formally documented test method and this might explain the differences between the assembly house (all were ok) and the test house results (6 STAR250 and 1 STAR1000 failed).
Later in the project a test was done with the perfluorocarbon test and no problems were reported.

3.3.1.7.2 Fine leak

The fine leak test is a He trace test (MIL-STD-883 method 1014 condition A). The required fine leak rate is 5.10^{-7}. No failures are reported.

3.3.1.8   Marking and serialization
All devices pass. The type variant and testing level is not indicated, because this can only be done after testing and the devices are marked at the start of the assembly.
Marking is defined as:
> "type"
> "serial number"
> "assembly date code"

Example:
> STAR1000
> 000118
> 02-02-2004

3.3.1.9   Materials and finishes
The outgassing properties of the used epoxy materials were tested conform to ECSS-Q-70-02
> The pass/fail criterion is:
> TML: max 1%
> CVCM: max 0,1 %

Epoxy	TML [%]	CVCM [%]
Die bond epoxy	1,101 ± 0,060	0,004 ± 0,004
Glass lid epoxy	0,842 ± 0,010	0,007 ± 0,006

The die bond epoxy is marginally out of spec. This was accepted.

3.3.2   Initial measurements (P6)
Initial measurements were performed on both STAR250 and STAR1000 at room temperature, -40 °C and +85 °C. The following parameters are measured:
- Power consumption (stand-by, total, image core, ADC)
- Offset and gain of different gain settings
- ADC ladder network resistance, INL and DNL
- Vsat
- Response in blue, green and red
- Noise, local FPN and global FPN at nominal speed, high speed and low speed
- Column FPN
- Dark signal, local DSNU and global DSNU
- Local PRNU and global PRNU
- # FPN defects, # DSNU defects, # PRNU defects

The results were used to set the specs and testing limits for the FM devices.
The results were as expected with the following exceptions: the STAR1000 dark current was significantly lower than expected (3135 e-/s expected, 785 e-/s measured). This has 2 main causes:
- The die temperature of the sensor was not monitored during previous testing in the development project of the sensor. This means that the expected value set from these results was too high and that the real value is indeed much better.
- The measurement was done with a rather low signal level in the non-linear part of the dark current. This means that the measured value is too low.

An additional verification in our lab shows that the real DC value is about 1.5 times the measured value on the test system. This factor has been used to set the specs to 1180 e-/s [average].

3.3.3   Evaluation

3.3.3.1   Control group (Group1)

A control group has been set. These devices have been measured together with the stressed devices at each intermediate of final electrical/electro-optical test. This allows excluding common cause problems such as test set-up issues.

3.3.3.2   Destructive tests (Group 2)

Destructive tests are intended to result in permanent damage of the sensor, and are therefore performed on a representative number of samples.
The following destructive tests are performed:
- Temperature step stress test
- Radiation tests
  - Total dose radiation
  - Proton radiation
  - Heavy ion radiation (SEE)
- Constructional analysis
- Package tests (mechanical, thermal, environmental)
- Electrical tests (ESD, power supply, thermal)

3.3.3.2.1   Temperature step stress test (Subgroup 2A)

The purpose of this test is to perform a thermal characterization and to define the thermal conditions for the accelerated endurance test by gradually increasing the temperature until the devices fail.
The thermal characterization on 5 devices each resulted in a junction-to-case thermal resistance of 5.1 °C/W for STAR250 and 3.6 °C/W for STAR1000.
The temperature step stress test (on 5 devices of each) is a biased test, where the devices are biased in an oven at certain temperatures. After each stress, the devices are tested electrically at room temperature and fine and gross leak tests are performed. The devices are stressed at +125 °C, +150 °C and +175 °C for 168h. Due to problems with the test fixtures at high temperatures, no stresses above +175 °C were performed.
Electrical tests showed no failures after each of the stresses. Leak tests showed fine and gross leak failures above 125 °C. This is explained by the fact that the glass lid epoxy has Tg of +124 °C. It was chosen not to change the epoxy for the time being. As a result of this there are some restrictions on device manipulation and assembly:
- Absolute maximum temperature (storage and operation) is below 124 °C
- No wave or re-flow soldering is allowed, only hand soldering
- De-golding and tinning has to be done manually, pin per pin.

3.3.3.2.2   Radiation tests

The purpose of the radiation test campaign was to execute a complete radiation test on the STAR1000 and to fill up the gaps in the already existing STAR250 radiation test results.
For STAR250 the PHD thesis work Of Dr. Jan Bogaerts already contained very good data. It was decided however to repeat the total dose irradiation on a larger number of samples and to complete the measurements with heavy ion radiation tests.
For STAR1000 only a brief total dose irradiation test was executed with unreliable results, due to manipulation errors. A complete test was organized containing total dose, proton and heavy ion irradiation.

3.3.3.2.2.1   Total dose

The total dose irradiation tests of STAR250 and STAR 1000 devices were based upon ESA basic specification ESCC 22900: Total Dose steady state irradiation method. More specifically, the "lot acceptance" method was applied.

The irradiations were performed at the ESTEC Cobalt 60 irradiation facility in Noordwijk (NL) from 23 February until 27 February 2004. The subsequent annealing at room temperature and at elevated temperature was done at FillFactory from 27 February until 11 March 2004.

A second irradiation test was performed on STAR1000 devices from NN August until NN August 2005.

The hardware, firmware and software to bias the components during irradiation and to perform intermediate electrical measurements were developed by FillFactory.

The STAR250 devices were irradiated up to a total dose of 254 Krad at a dose rate of 2.66 Krad/hr.
The STAR1000 devices were radiated up to 291 Krad at an average dose rate of 3.05 Krad/hr.

During irradiation the devices were powered on and biased to nominal conditions. All digital inputs were fixed to the nominal, stand-by state except for the X-clock and ADC clock. The signals were continuously clock at a reduced clock rate (10 KHz) in order to keep the devices in a known state.

The tests showed a number of remarkable results and observations:

- Average dark current rise during irradiation

- Average dark current rise during annealing

- A large spread between the samples

- Dark Current increases for all pixels almost equally, no additional hot spots

- Average DSNU rises with the irradiation dose

- The average DSNU remains constant during annealing

- The spread in DSNU between samples decreases during annealing at temperature

The following paragraphs elaborate some of these observations in more detail.

3.3.3.2.2.1.1 Average dark current rise during irradiation:

The average dark current rise during irradiation amounts to 219 e-/s per Krad for STAR250 and 252 e-/s per Krad for STAR1000. This result is comparable to what was observed during earlier tests. .
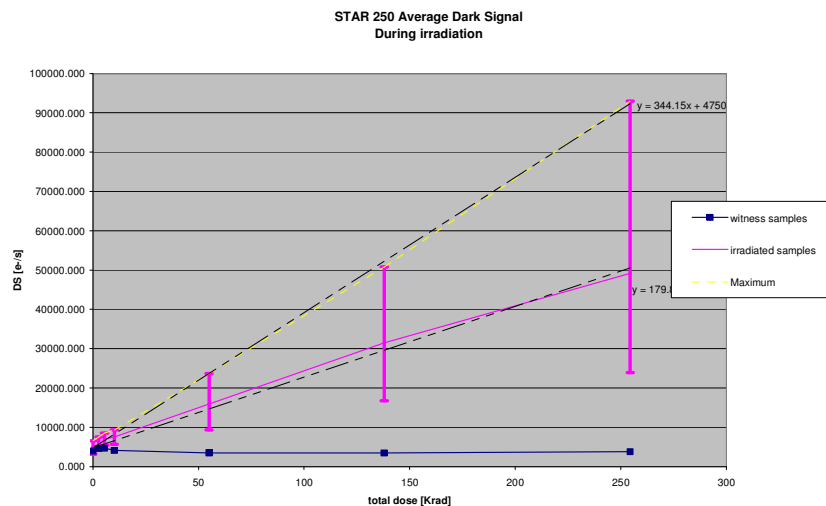
Figure 13.   STAR250 average dark current during irradiation

3.3.3.2.2.1.2 Average dark current rise during annealing and large spread between samples.

The average dark current still rises during annealing: 130 e-/s per Krad for STAR250 and 221 e-/s per Krad for STAR1000.

However is was observed that devices that showed a relatively large increase in dark current during irradiation only showed little or no increase or even slight decrease during annealing, while

devices that showed less increase during irradiation, still showed dark current rise during anneal. As a result, the large spread between devices immediately after irradiation is significantly reduced after annealing.

Earlier tests did not show this effect but they were done on a very limited number of samples (2). The exact mechanism behind these phenomena is still unclear but it is assumed that the unrealistically high dose rate of the tests can explain the strange behavior.

From these tests it was learned that in the future, total dose testing must be conducted at much lower dose rates in order to obtain reliable results. Moreover, the device specification of the STAR250 and STAR1000 will contain the worst-case test results as radiation tolerance specification.
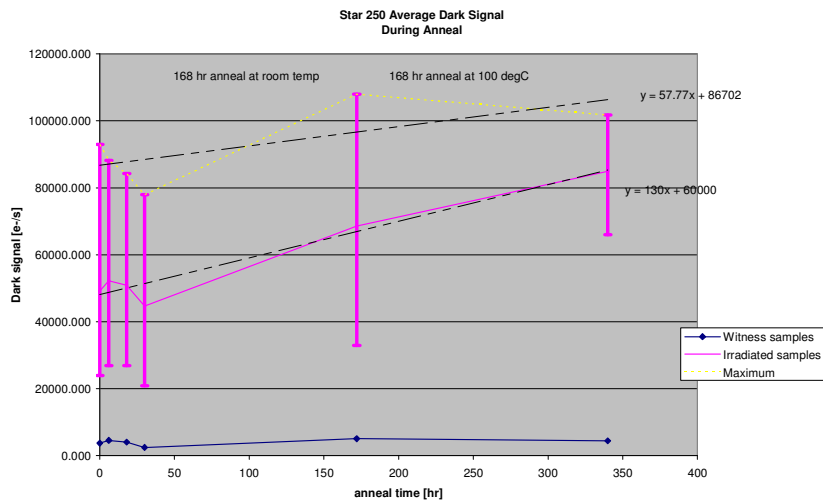
Figure 14.   STAR250 average dark current during annealing

3.3.3.2.2.1.3 The average DSNU rises with the irradiation dose but no hot spots were observed
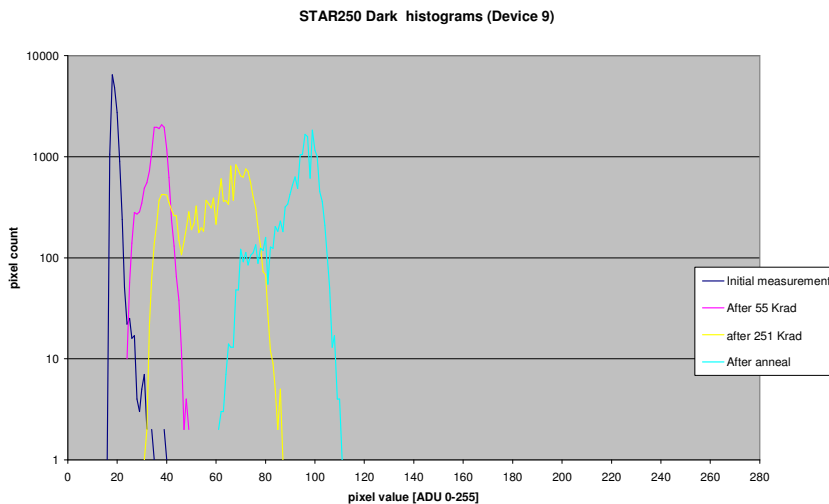
During irradiation, the average DSNU rises with 58 e-/s per Krad for STAR250 and 6 e-/s per Krad for STAR1000.

The histogram over a dark image, taken during irradiation and annealing shows that the average dark current rises: the histogram peak moves to the right. The DSNU also rises during irradiation: the histogram becomes wider. During annealing the dark current rises further but the DSNU

remains constant: the histogram width remains the same. No additional hot spots are observed during irradiation or annealing.

3.3.3.2.2.1.4   The spread in DSNU between samples decreases during annealing.

This behaviour is similar to the average dark current behaviour and can probably also be explained by the high dose rate at which the tests were conducted.

-
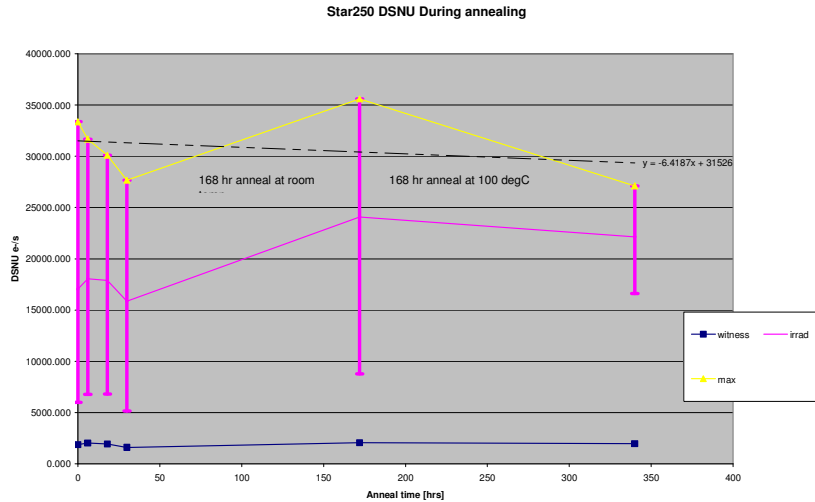
3.3.3.2.2.2   Proton irradiation

Proton irradiation tests on STAR250 were performed previously, therefore only STAR10000 was tested for proton irradiation. 9 samples and 3 witness samples were used for this test. The irradiations were performed at the irradiation facility of the Universite Catolique de Louvain (UCL) facilities on March 5, 2004.

The devices were divided into three groups, each irradiated at different energies: 10MeV, 30 MeV and 60 MeV. Within each energy-group, the three devices were irradiated during an increasing time (30 s, 180 s and 600 s) such that measured parameters like dark current and DSNU could be related to both particle energy and total fluence. Thus the applied fluence amounted to 2.4 E10, 7.2E10 and 2.4E11 protons/cm2.

During irradiation the samples were not biased, all connections of all devices were connected to GND.
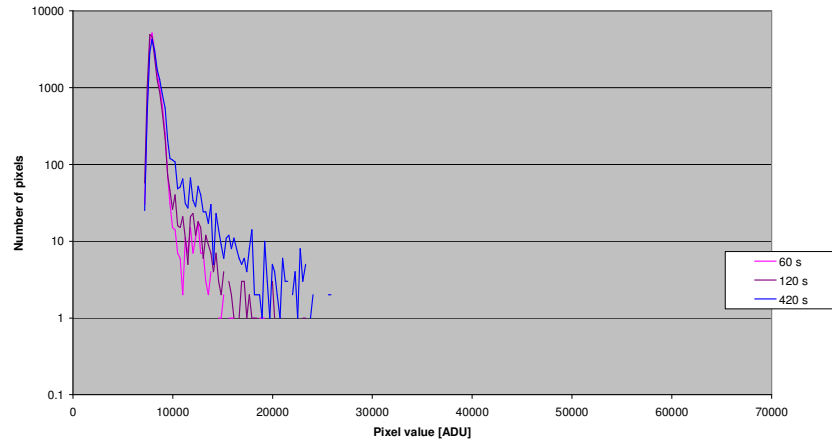
No significant influence was observed for:

- Power consumption

- FPN

- Number of FPN defects.

An expected increase was seen for:

- Average Dark current (x2.5)

- DSNU (x3)

- Number of DSNU defects (x500)

Dark Signal image histograms of device 97
after proton irradiation at 60 Mev

The histogram shows that, although the peak value of the dark current stays at the same location, the tail into the higher values increases with increasing fluence. This results in a higher average value ant a higher DSNU. This effect is more prominent at higher energies.

3.3.3.2.2.3 SEU

Both STAR250 and STAR1000 were tested for single event upset by irradiating them with heavy ions. The irradiations were performed at the irradiation facility of the Universite Catolique de Louvain (UCL) facilities on March 10 2004.

1 sample of each was irradiated with two different ion beams: Ar with an energy of 150 MeV and Xe with an energy of 459 MeV. The samples were irradiated with incidence angles of 0 deg and 60deg, the latter doubling the effective Linear Energy transfer (LET). By doing so the samples were tested at the following LET values: 14.1 28.2 55.9 and 111.8 MeV cm2 / mg.

During irradiation the samples were operated at nominal frequency in the irradiation chamber. A dedicated system was built to monitor the power supply current on each power supply line and to cut the supplies in the event of a latch-up. This way, the power supply connection where latch-up would occur could be identified. Moreover, the system allowed storing a sequence of 200 subsequent images for the STAR1000 and 800 images for the STAR250 during irradiation.

Images were taken at 2 different integration times: the shortest possible (1 line time) and at full frame time.

Susceptibility to latch-up:

During these tests no latch-up condition occurred. In the worst case condition both sensors sustained a total dose of 10E7 particles with an effective LET of 111.8 MeV/mg/cm2**.**

Influence on image quality:

During the different irradiation sessions image sequences were taken. It was observed that the impact of heavy ion particles causes temporary saturated white spots at the location of impact on the sensor. The size of these spots are in the order of 2 to 3 pixels at lower LET and grows with longer integration time to saturated white blobs of 5 to 10 pixels diameter at higher LET. The number of spots increases with integration time. All spots disappear at the next image and no permanent damage was observed.

3.3.3.2.3 Construction analysis

Construction analysis was performed by ESTEC on 3 samples of STAR250 and 3 samples of STAR1000. It consists of:

- External visual inspection
- Radiographic inspection
- Physical dimensions check
- Die alignment and lateral position

- PIND testing
- Hermeticity testing
- Pin Integrity
- RGA (Residual Gas Analysis)
- Internal Visual Inspection
- SEM inspection
- Bond strength test
- FIB analysis (Focussed Ion Beam)
- Microsection
- Materials analysis
- Die attach

The following conclusions are stated in the report:

- The primary packaging was thought inadequate to protect the parts from high G impacts in any direction
- Two of the die had particles on the surface which were considered to fail the special requirements of the manufacturer's documentation. In this instance, the limit for the maximum dimension of any particle was 20µm.
- The radiographic examination reveals an inadequate die attach coverage on serial number 104. The minimum limit for die attach is 50 percent."
- Residual gas analysis revealed a high water content"
- Internal visual examination showed the presence of bond wire tails that exceed the requirements of the Mil Spec with regard to their length. Bond wire tail length is, however, a lot related feature and bears little relevance to the reliability of the design. The observed excesses in this lot are also marginal."

Each of the issues was examined and a solution was defined:

- Primary packaging: this problem was also reported at the initial inspection (P5). This was recognised and in phase 2 a new tray was developed for the transport and storage of the parts. This tray provides a better protection.
- Particles on the die: the parts were inspected at the start of the evaluation, but they were not rejected for particles. The FillFactory inspection results confirm the results in the report. This shows that the inspection at FillFactory catches these defects and that they would be seen on FM products.
- Die attach coverage: this was also reported during the initial radiographic inspection (P5). This is discussed in paragraph 3.3.1.6 "Radiographic inspection".
- High water content: the RGA shows a water content of 12%, with the spec being 0.5%. It was not clear whether the analysis results are reliable or not. Therefore new samples were provided do to additional testing (STAR250 #178 and #174). These tests gave similar results. There are 2 potential causes for the high water content:
  - o The water is absorbed by the package, glass or epoxy during the gross leak test. The initial gross leak test was done with alcohol, but at the end of the project a test was done with perfluorocarbon (MIL-STD 883 method 1014 condition C) which does not contain any water. Therefore the gross leak test is considered not to cause the high water content. The test that was done at the end of the project was done with 45psi for 10 hours. The replacement of the gross leak test by a visual inspection will only be released after approval from ESA.
  - o The ceramic package contains a lot of water that is released at high temperature (RGA is done with a temperature step before testing). New test samples are assembled in phase 2 with a 1hour/125 °C bake-out before glass lid attachment. This gave 5% to 9% moisture inside which is still too high. A last series of test samples was produced with a 24h/125 °C bake-out before glass lid attachment. This resulted in a moisture level of 2%. This shows that a big part of the 12% moisture comes from the package, the remaining 2% is assumed to be outgassed by the glass lid epoxy during curing. This can only be improved by using another epoxy or another sealing method. The 2% is a big improvement and for the time being we have to live with it.

- Bond wire tail length: The specification is max 2x the wire diameter, and the products are marginally out of spec. This is an assembly process related issue. The process was improved in phase 2 with satisfactory results.

3.3.3.2.4   Package tests

The purpose of package tests is to test the assembly configuration (combination of package, die and glass lid) by stressing it thermally, mechanically and environmentally.

3.3.3.2.4.1   *Thermal cycling and Thermal shock*

Thermal cycling and thermal shock are done 100 cycles/shocks in stead of 10 (ESCC9020 qualification). However an intermediate test (electrical + fine and gross leak) is done after 10 cycles/shocks. The intermediate test shows whether the devices will survive the 9020 qualification requirements.
10 cycles + 90 cycles [-55°/+125°] were performed on 2 devices of each. Thermal cycling is done in a thermal chamber without biasing the devices. No failures or changed characteristics were noted.
10 shocks + 90shocks were performed on the same devices as the thermal cycling. For thermal shock the devices are immersed alternating in a cold and hot liquid. At the end some detached pins were noted but no changed characteristics were noted. This was considered to be a handling issue, and confirmed by a 2nd test after explaining the handling issues to the subcontractor.

3.3.3.2.4.2   *Moisture resistance*

For the moisture resistance test, the devices are kept in a moisture chamber with a cycling relative humidity (MIL-STD-883 method 1004). Afterwards the devices are tested electrically and for fine and gross leak. No failures were noted.

3.3.3.2.4.3   *Mechanical shock and vibration*

3.3.3.2.4.3.1   Test description

Mechanical shock and vibration are performed 10 times the required pulses/sweeps of ESCC9020, with an intermediate test/inspection after the ESCC9020 required number of pulses/sweeps.
The shock test is done on 2 samples of each by mounting the tested unit on metal block which is dropped from a specific height to reach the required shock level, which is 150g – 0.5ms – ½ sine, 5+45 shocks in 3 axes
The vibration test is done on the same 2 samples of each by mounting the tested unit on a vibration table. The vibration level is 20g – max 0.06 inch, 4+36 sweeps in 3 axes.

3.3.3.2.4.3.2   Test 1

The clamping of these devices was considered as a problem for the mechanical tests. Therefore the subcontractor that did the tests used the shipping tray to hold the devices. This is not a suitable clamping method to withstand high G forces, resulting in loose pins and devices shaking around in the tray. 1 STAR250 device was completely destroyed. The devices that survived were electrically ok.

3.3.3.2.4.3.3   Test 2

A new test was started with 4 STAR250 devices each glued and soldered on a PCB. No failures were noted after vibration testing. After the 2nd cycle of mechanical shocks all devices fail due to broken pins and pins that have cracks in the soldering. This is caused by the flexibility of the pcb and the fact that the pins were not de-golded before the soldering. No broken packages or broken glass lids were noted. Based on the facts that mechanical shock was successful on STAR1000 in the first test, and vibration was successful on the pcb mounted test, the mechanical testing is considered to be successful. However an additional test with a proper test fixture was performed (see test 3).

3.3.3.2.4.3.4   Test 3

A mechanical test fixture was developed. This is a metal stud which is glued on the back of the tested sensor. This stud was fixed to the vibration table and shock block with a basic metal structure (see photos).
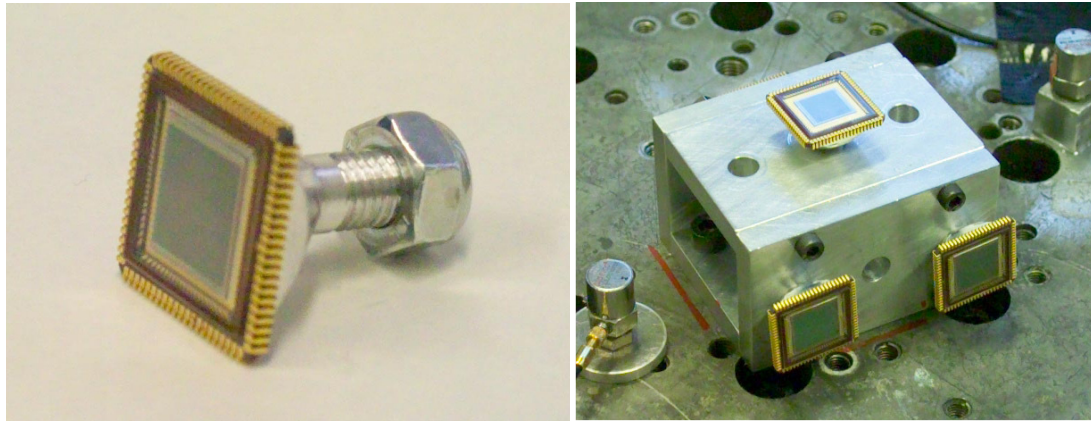
This fixture allows electrical testing afterwards, since the sensors are facing down in the tester. 2 STAR250 devices and 2 STAR1000 devices are tested. No failures were noted after vibration. For the shock, the STAR1000 devices showed no failures but the STAR250 devices showed a broken glass lid. The reason for the broken glass lids is not known, but it is assumed that the mechanical test requirements are too severe for a sensor with a glass lid on top.

The results of the mechanical testing show that the mounting of the sensors in an application has to be done with care. Soldering should be done conform to space requirements and the sensor should be fixed by gluing the back to a fixed structure.

3.3.3.2.4.4   Solderability

In this test the solderability of the pins using tin lead eutectic solder is verified (MIL-STD-883 method 2003). 3 STAR250 and 3 STAR1000 were tested. No failures or problems were noted. However wave or reflow soldering is allowed due to the thermal restrictions of the glass lid epoxy (see paragraph 3.3.3.2.4.7 "resistance to soldering heat").

3.3.3.2.4.5   Marking performance

The marking performance test verifies the resistance to solvents of the marking on the backside of the sensor (ESCC 24800). 3 STAR250 and 3 STAR1000 were tested. No failures or problems were noted

3.3.3.2.4.6   Terminal strength

The terminal strength test verifies the mechanical strength of the pins and the resistance to metal fatigue by applying a repeated bending of the pins (MIL-STD-883 method 2004 condition B2). 3 STAR250 and 3 STAR1000 were tested. No failures or problems were noted

3.3.3.2.4.7   Resistance to soldering heat

The resistance to soldering heat test consists of a soldering dip during several seconds. This test was done on 1 STAR250 and 1 STAR1000. Both parts had the glass coming off during this test. Electrically both parts were ok.

This is caused by the test method, which is a soldering dip. A test with manually soldered devices caused no failures, even after fine leak and gross leak testing. A manual soldering requirement was taken up in the detailed specifications [AD01, AD02].

3.3.3.2.5   Electrical tests

3.3.3.2.5.1   ESD sensitivity

5 samples of each are tested for HBM ESD. Both STAR250 and STAR1000 are ok at 250V and start failing at 300V. The most sensitive pins are:

STAR250: VHIGH_ADC; VLOW_ADC; D0-D9; VDD_ADC_DIG_3.3/5; GND pins

STAR1000: VHIGH_ADC; VLOW_ADC; VDD_DIG_OUT; VDD_ADC_ANA

Both are classified as class 1A (JEDEC classification) product. The means that all handling has to be done with care:

- Always manipulate the devices in an ESD controlled environment
- Always store the devices in a shielded environment that protects against ESD damage
- Always wear a wrist strap when handling the devices and use ESD safe gloves.

3.3.3.2.5.2   Characterization vs. power supply voltage

The devices are tested between 2.5V and 6.5V in 0.5V steps. Both products operate well between 4V and 5.5V. Outside these values the sensors are still working but several parameters are out of spec (also because the pass/fail limits are not changed with the voltage). The use of alternative voltages is to be avoided.

3.3.3.2.5.3   Characterization vs. temperature

4 STAR250 and 5 STAR1000 are tested between -40°C and +120°C in 20°C steps. Figure 15 and Figure 16 show the dark signal results.
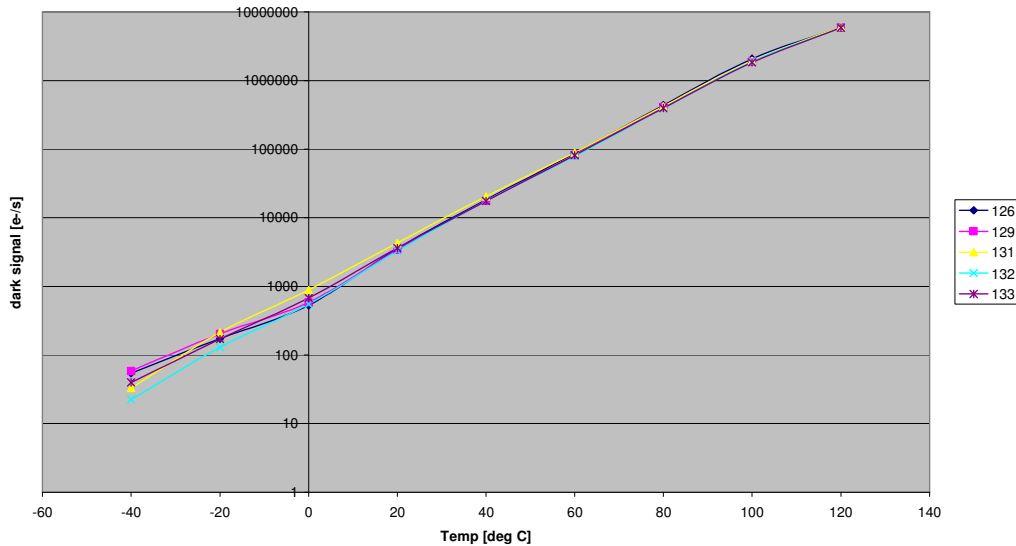

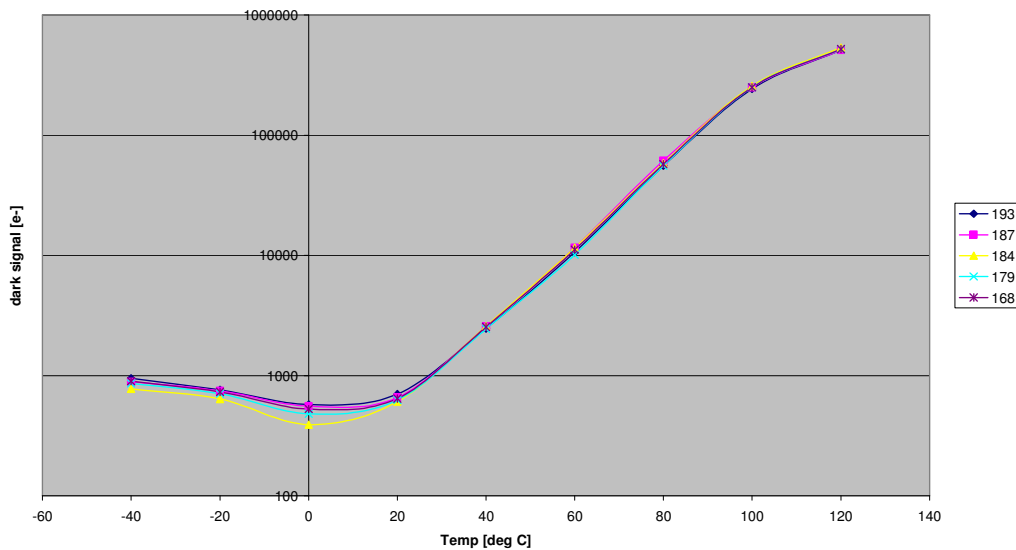*Figure 15.   STAR250 dark signal vs. temperature*

Figure 16.   STAR1000 dark signal vs. temperature

STAR250 dark signal as function of temperature shows a very linear curve, with the sensor reaching its non-linear behaviour (near saturation) at 120 °C. This results in a dark signal that doubles every 9,0 °C.

STAR1000 dark signal as function of temperature shows a linear behaviour between 20 °C and 80 °C. At 100 °C the sensor is reaching its non-linear behaviour (near saturation). Below 20 °C the dark current shows a minimum around 0 °C and a slightly increasing dark current below 0 °C. The linear part of the graph results in a dark signal that doubles every 9,2 °C. It is assumed that the increase at low temperatures is a side effect of the test method but there is no specific explanation for it. At room temperature dark current is measured using an integration time of 10 frames, which results in sufficient dark signal for a significant measurement. Using an integration time of 10 frames at -40 °C results in not enough dark signal for a significant measurement, however an increase of the integration time to 100 frames results in enough signal, but the dark current result is about the same as at room temperature. This looks like a contradiction because if the measurement at -40 °C is correct, it should give enough dark current for a significant measurement.

An increase of DSNU and #DSNU defects with temperature was noted. This was as expected/
There is a small increase in power consumption at low temperatures, caused by the ADC. There is no clear explanation for it, but the increase is smaller than 10% and therefore not considered to be a problem.

The temperature range of the products was set to -40°C/+85°C [AD01 and AD02]. The high limit is based on:

- The non-linear behaviour above 100°C
- The thermal restrictions of the glass lid epoxy

3.3.3.3 Endurance tests (Group 3)

An endurance test was executed on 15 devices of each type, at 125 °C for 2000h with intermediate measurements at 168h, 500h and 1000h.

6 samples were measured electro-optically before and after the test:

- Spectral response
- Electro-optical response
- MTF

The STAR1000 test had to be restarted due to a failure after 168h on all devices. The devices had an electrical overstress caused by the biasing equipment. The test was restarted with spare devices.
No failures were observed at the 2000h endurance test. Taken into account the standard deviation of the test results, no significant changes were observed in any of the characteristics.

3.4 Screening

A screening procedure for FM sensors was defined and is taken up in the detailed specifications [AD01 and AD02]. The screening consists of:

- X-ray
- PIND test
- Stabilization bake 48h at 85°C
- Temperature cycling: 10 cycles -40°C/+85°C
- Burn in 240h at +85°C
- Electrical measurements at room temperature, +85°C and -40°C
- Fine and gross leak test
- Visual inspection

3.5 Conclusion

The overall conclusion is that both STAR250 and STAR1000 are suitable candidates for qualification for use in space application. On the design of the products the glass epoxy performance is subject to improvement and would benefit from further investigation or selection of a different epoxy. On the testing side there were issues with test methods that were not suitable for an image sensor, resulting in a series of retesting and suitable test methods being found and implemented. The transport container was also redesigned in order to prevent the pins from being bent.

The data of this evaluation program has been used to update the detailed specifications. The latest versions at time of writing this report are:

- STAR250 detailed specification version 2.0
- STAR1000 detailed specification version 2.0

These detailed specifications can be obtained at ESA or directly at Cypress Semiconductor Belgium BVBA.

An EPPL entry application was filed.

4 Development of HAS/LCMS

4.1 HAS

The aim of the HAS APS sensor was to develop a new high end space sensor to enable a highly accurate STR. By 'high accuracy' a noise level (from the STR) of less than 1 arc-second is intended. In order to reach these accuracies, a large number of pixels are combined with a relatively small sensor field of view (FoV). With the small FoV, there must still be sufficient stars present to be able to perform tracking and attitude determination, hence the sensitivity of the device has been increased and the noise floor (which determines the star detection limit) had to be decreased compared to the existing STAR-1000 device.

Figure 17 shows the architecture of the HAS sensor. The pixel pitch is 18 µm (15 µm for STAR-1000). The sensor integrates a 1024 x 1024 pixel array, a dual addressable y shift register for rolling shutter operation, programmable offset and gain amplifier and an on-chip 12-bit pipelined ADC.
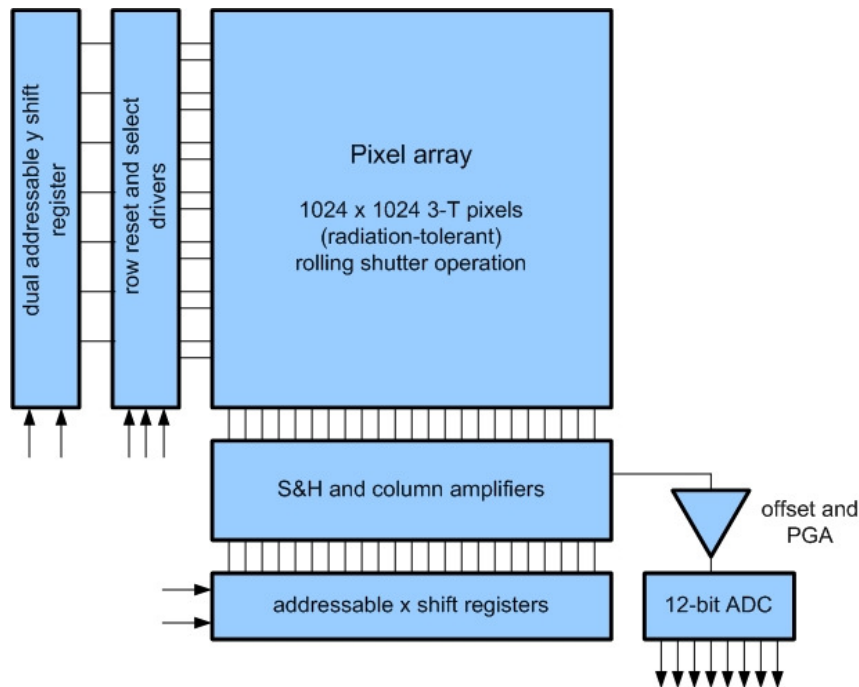
Figure 17.   Simplified HAS architecture.

The sensor can also be read out non-destructively, i.e. the pixel is reset and afterwards sampled and readout two or several times without additional reset in between. This mode of readout, which could not be achieved in the STAR sensors, is schematically depicted in Figure 18. The initial reset level and all intermediate signals can be recorded. High light levels will saturate the pixels quickly, but a useful signal is obtained from the early samples. For low light levels, one has to use the later or latest samples. The external system intelligence should take care of the interpretation of the data. Since all data points are from the same reset cycle, they all exhibit the same reset noise. Therefore, this operation mode leads to the lowest possible read noise, either by off-chip curve fitting techniques or by basic off-chip correlated double sample subtraction (CDS). In the latter case, the reset level is simply subtracted from the single level after a given integration period.

Figure 18.   Non-destructive readout operation.

The whole sensor is designed using proprietary techniques to achieve high radiation tolerance (currently tested up to 100 krad(Si)). The HAS sensor has been processed in the 0.35 μm 1P3M XFAB technology.

4.1.1 Design description

4.1.1.1 Floor plan
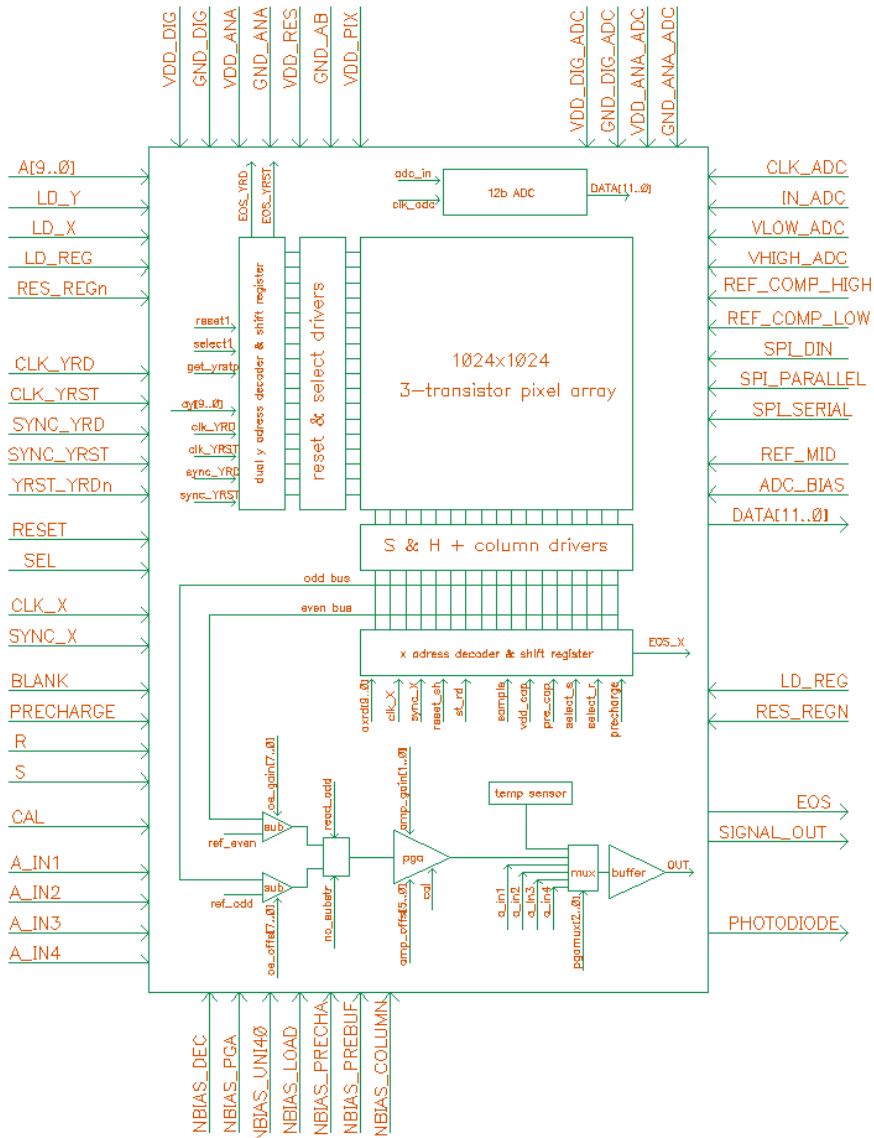
Figure 19.   HAS floor plan

Figure 19 shows the architecture of the image sensor that has been designed. It consists basically of the pixel array, shift registers for the readout in x and y direction, parallel analog output amplifiers, and column amplifiers that correct for the fixed pattern noise caused by threshold voltage non-uniformities. Reading out the pixel array starts by applying a y clock pulse to select a new row, followed by a calibration sequence to calibrate the column amplifiers (row blanking time). Depending on external bias resistors and timing, this sequence takes about 5 µs per line. This sequence is necessary to reduce the Fixed Pattern Noise of the pixel and of the column amplifiers themselves (by means of a Double Sampling technique). DACs have been added to make the offset level of the pixel values adjustable. A

12-bit ADC running at maximum 10 Msamples/s can optionally be used to convert the analog pixel values.

4.1.1.2 Pixels

In an early stage of the program, a large number of pixels have been designed and tested. Examination of their performance resulted in the selection for this sensor of an 18 micron three transistor radiation-tolerant pixel.

A square array contains 1024x1024 three-transistor linearly-integrating pixels. Each pixel has a connection for a reset line, for power, an output select line, and eventually the pixel's output signal.

Figure 20.   Three-transistor pixel. Transistor-level diagram (left),
and functional equivalent (right).

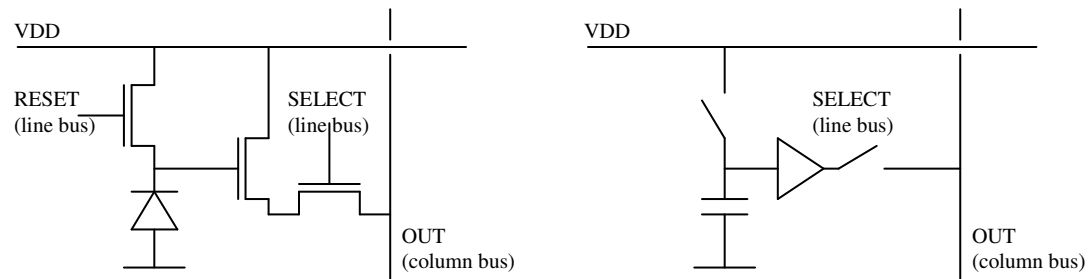There are three transistors in a pixel. The first one acts as a switch between the power supply and the photodiode. The photodiode is equivalent to a capacitor with a light-controlled current source. The second transistor is a source follower amplifier, buffering the voltage at the photodiode/capacitor cathode for connection to the outside world. The third transistor again is a switch, connecting the output of the buffer amplifier to an output signal bus.

Due to asymmetry in the metal interconnections op top of the pixel, the pixel profile of the STAR-1000 is highly asymmetric and charges are spread over a larger number of pixels. Special care has been taken to organize the pixels and to layout the metal routing of the HAS pixels in such way that the pixel response is very symmetrical (see further).

4.1.1.3 Peripheral circuits

4.1.1.3.1 Column sample & hold capacitors

Under every column of pixels two capacitors are located for sampling the reset and signal levels of the selected pixel. In previous designs of FF, both sampled levels suffered from cross-talk to each other. This resulted in less FPN correction performance. The sample and hold design of the two capacitors is changed to improve the FPN correction.

In non-destructive read-out, both sample capacitors are still used. Both capacitors contains after sampling the same signals. The read-out sequence is the same as in destructive read-out but only the signal coming from the signal sample-capacitor is used. The subtraction circuit and PGA ignore the reset signal coming from the pixels.

4.1.1.3.2 Column amplifiers

Under every column of pixels sits one column amplifier, for writing the hold signals on the S&H capacitors to the output channel. In destructive read-out the reset and signal levels are subtracted in the output amplifier canceling most of the fixed pattern noise. In non-destructive read-out, only the signal level is used by the output amplifier.

4.1.1.3.3   Row and column selection logic

A required feature is the full addressability of rows and columns. There are two Y shift registers called YRST and YRD and one X registers called XRD. The user can sync these shift registers at any X-Y position. At each Y clock cycle, the two Y pointers shift to the next position to read/reset the next row(s), i.e. enabling the rolling shutter readout of the pixel array. The integration time is determined by the difference in position of the two pointers. For more details, see [ICD1].

4.1.1.3.4   Output amplifier

The output amplifier has been designed for 10 MHz pixel rate. It contains 4 electrical blocks:
- Subtraction logic: in this block the photo-signals and reset levels of the pixels are subtracted in case of double sampling mode. In NDR, the reset levels are substituted by a DC level that can be set by the BLACK register (see next paragraph). As can be seen in Figure 19, the signals from the odd and even columns are multiplexed. A difference in offset can be balanced using the OFFSET register (see next paragraph).
- Programmable gain amplifier: in the gain amplifier, the offset of the analog signal is set (AMP register). The gain amplifier can be set in 4 gain modes.
- Input signal multiplexer: the multiplexer can be set to multiplex either the analog signals from the pixel core, the on-chip temperature sensor or one of the four analog inputs.
- Output buffer

4.1.1.3.5   On chip registers

There are six registers on the chip, which control the operation of the device. In the table below, the names en functionalities are listed.

name	Size	Reset value	Description
X1	10 bit	'0000000000'	Start position of XRD shift register
Y1	10 bit	'0000000000'	Start position of YRD and YRST shift register
MODE	8 bit	'00000000'	End of scan multiplexer, PGA multiplexer, NDR or DR mode, standby or active mode
AMP	8 bit	'00000000'	Output offset and gain of PGA AMP[7..2] = offset of PGA AMP[1..0] = gain of PGA
BLACK	8 bit	'00000000'	Black signal reference for NDR
OFFSET	8 bit	'00000000'	Offset correction between odd and even columns

4.1.1.3.6   Digital to analog converters

There are 3 DACs (see AMP, BLACK and OFFSET registers) for generating 3 different biasing voltages. The biasing voltages generated by these DACs are used in the output amplifier and for pre-charging the column structures.

4.1.1.3.7   Temperature sensor

A temperature sensor based on a forward biased p+/n-well junction diode is integrated on the chip. The resultant temperature-proportional voltage can be routed to the ADC through one of the six analogue inputs of the multiplexer. The temperature sensor must be calibrated on a device-to-device base (for measurement results, see further).

4.1.1.3.8   Analogue to digital converter

The on-chip ADC is a 12 bit pipelined converter. It has a latency of 6.5 ADC clock cycles, i.e. it samples the input on a rising clock edge, and outputs the converted signal 6 pixel clock periods afterwards on the falling edge. When the first stage of the ADC is sampling the value at the input of the ADC, the following stages are processing previous values. The ADC runs at the same rate as the pixel readout rate.

The ADC is electrically isolated from the actual sensor core: when unused it can be left non-powered for lower dissipation. The ADC has proven to be radiation tolerant and is designed by using the same radiation hardening layout techniques as used in the HAS image sensor.

4.1.2 Test plan

The following tests have been performed on the HAS image sensor:
- ADC
  - Set-up and hold time
  - Delay time
  - Linearity
  - Power consumption
- Electro-optical characterization (mainly at room temperature)
  - Spectral response
  - Photo response and photo response non-uniformity (PRNU)
  - Dark current (DC) and dark current non-uniformity (DCNU) (also as function of temperature)
  - MTF and pixel profile
  - Noise (temporal and fixed pattern noise (FPN)) (also as function of frequency)
  - Power consumption
  - Anti-blooming
  - Temperature sensor (as function of temperature)
- Total dose radiation

4.1.3 Requirements

This section lists the requirements posed to the HAS. These requirements originate both from ESTEC's initial analysis as well as a number of early design decisions based on the architecture and operational modes (e.g. Non Destructive Readout with digital Correlated Sampling, windowing, ...).

4.1.3.1 Functional requirements

No.	Requirement
F1	The sensor shall provide a measure of the amount of signal (electrons) in each pixel as a digital count with 12 bit accuracy.
F2	The Gain and Offset of the on chip ADC shall be dynamically settable.
F3	The sensor shall be capable of reading the entire pixel array (one frame) every 200ms
F4	The sensor shall be capable of reading out 40 windows of 20*20 pixels (each) every 100 ms
F5	The sensor shall be capable of supporting adjustable pixel integration times with a given fixed readout time. (e.g. 10Hz readout rate with pixel integration times of 5 to 100ms per pixel)
F6	Sensor shall be capable of supporting window to window variable ADC (gain and offset) setting.
F7	The on chip ADC shall be able to accept and digitise up to 4 externally provided analogue signals.
F8	The HAS shall have a temperature monitor on chip.
F9	The HAS shall be able to be operated in (Non Destructive Readout) NDR and (Destructive Readout) DR modes – as dynamically selected by the user

4.1.3.2 Performance requirements

No.	Requirement
P1	At BOL (i.e. zero radiation dose) the Dark Current shall be less than 2500e/pixel/second at 25 degrees Celcius.
P2	At EOL (i.e. full radiation dose) the Dark Current shall be less than 5000 e/pixel/second at 25 degrees Celcius.

P3	The sensor readout noise (including KTC Noise) shall be less than 30 electrons/pixel (1 sigma value over time and all pixels) at EOL.
P4	Cross Talk is defined as the % of the signal in one pixel that appears as a parasitic signal in a neighboring pixel. The Cross Talk shall be less than 8% and shall be invariant over life.
P5a	For DR, the Fixed Pattern Noise (FPN) shall be less than 45 electrons (1 sigma over any 10*10 pixel sub-array) at EOL.
P5b	For NDR, the residual FPN shall be less than 10 electrons (1 sigma over entire detector array) at EOL
P6	The Pixel Response Non Uniformity (PRNU) shall be less than 1.5% over the entire pixel array and less than 0.25% over any 5*5 sub-array of pixels.
P7	The Dark Current Non Uniformity (DCNU) shall be less than 5% at EOL (1 sigma over all pixels). The BOL and EOL DCNU distribution over the detector shall be provided.
P8	The sensor shall have a response that is linear to within 5 % over the range 0 – 80,000 electrons/pixel and which shall be fixed over life. For signal levels up to 120,000 electrons/pixel, the effects of nonlinearity shall be calibratable to better than 1%
P9	The sensor shall have a sensitivity (defined as Fill factor * Quantum Efficiency) of greater than 40%. (Goal: Greater than 70%) average over the spectral range.
P10	The sensor shall have an anti-blooming capability of at least 1000 times the full linear range.
P11	The spectral range of the sensor shall at least cover the wavelengths 0.4 to 0.9 microns.

4.1.3.3 Physical characteristics

No.	Requirement
C1	The sensor shall be compatible with Pixel Array sizes of 768*768 to 1024*1024 pixels. The baseline array size shall be 1024*1024 pixels.
C2	The sensor active area shall be less than 19 * 19 mm
C3	The pixel dimensions shall be determined by the Contractor in order to comply with requirement C2 and the performance requirements but shall be greater than 14 microns along each side.
C4	The sensor power consumption shall be less than 300 mW at EOL and full speed operation. (Goal: 150mW)

4.1.3.4 Environmental characteristics

No.	Requirement
E1	The sensor End of Life (EOL) condition is defined as 15 years continuous operation in vacuum after being subjected to vibrations specified in Requirement E5 and the radiation dose specified in Requirement E6
E2	The sensor shall be compatible with an operating temperature range of –35 to + 40 °C
E3	The sensor shall be compatible with a non-operating temperature of –40 to + 100 °C
E4	The sensor shall be compatible with either a 3.3v or a 5v single power supply.
E5	The sensor shall be able to survive and operate nominally after being subjected to a random vibration for a duration of 2 minutes: • 20 –100 Hz +3dB/Oct • 100 – 300 Hz 2.4 g_2/Hz • 300 – 2000 Hz -5 dB/Oct
E6	The sensor shall be able to survive and operate nominally after being subjected to a total ionizing dose of 150Krads.
E7	The sensor shall be Single Event Latch up free under radiation with a Linear Energy Transfer spectra specified below: TBD
E8	The sensor shall be able to survive, without damage, a shock corresponding to 2000g for a 1000Hz half sine wave.

4.1.4   Test results

This section summarizes the most important test results and measured electro-optical behavior of the HAS sensor.

4.1.4.1   ADC

The test set-up that was used was not accurate enough to give a decent INL and DNL measurement. The accuracy of the measurement of the input voltage was too low and the granularity of the stepwise input voltage needs to be improved. The test setup was also not able to do a noise measurement on the 12 bit ADC. Apart from there limitations by the measurement set-up, capacitor mismatch and reference code dependency results in characteristic jumps of at least 2 LSBs in INL curve.

Figure 21 shows the output code deviation from a linear fit. It is clear that the ADC does not reach the 12 bit accuracy at 5MHz sample rate. The real accuracy of the ADC is around 10 Bit. When operating at 1 MHz, the ADC is more linear at the lower and higher codes. The jumps are all downwards. This means that the internal gain of the stages is too large and that a lower gain will probably increase the INL performance. Uploading a different calibration code can reduce the internal gains.
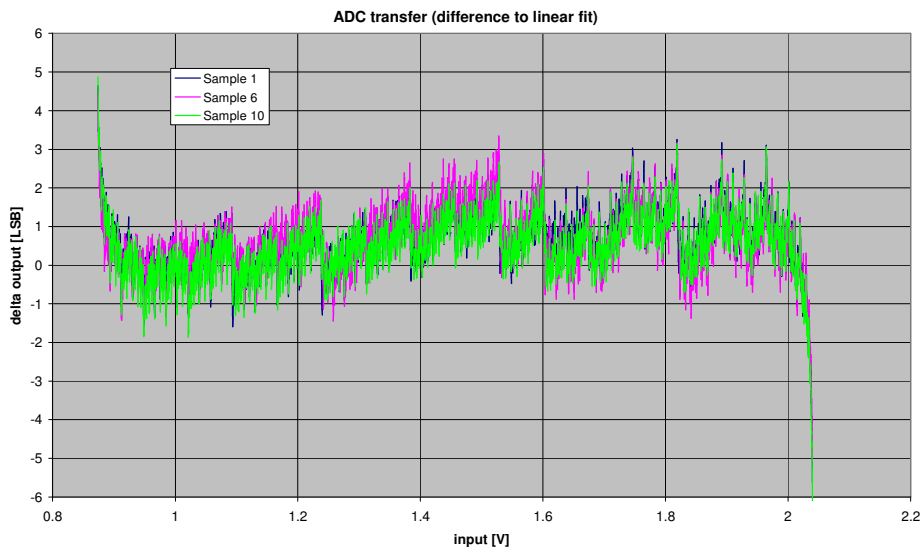
Figure 21.   Output code deviation from a linear fit (at 5MHz operation).

4.1.4.2   Spectral Response

Figure 22 shows the quantum efficiency, including the fill factor, of the STAR-1000, the STAR-250, the HAS and LCMS sensors. The average quantum efficiency for the wavelength range of 400 to 720 nm is respectively 22%, 29%, 40% and 43%. The quantum efficiency obtained on the two new sensors is approximately the largest that can be achieved for front-side illuminated devices taking into account the metal fill requirements imposed by the CMOS foundries.

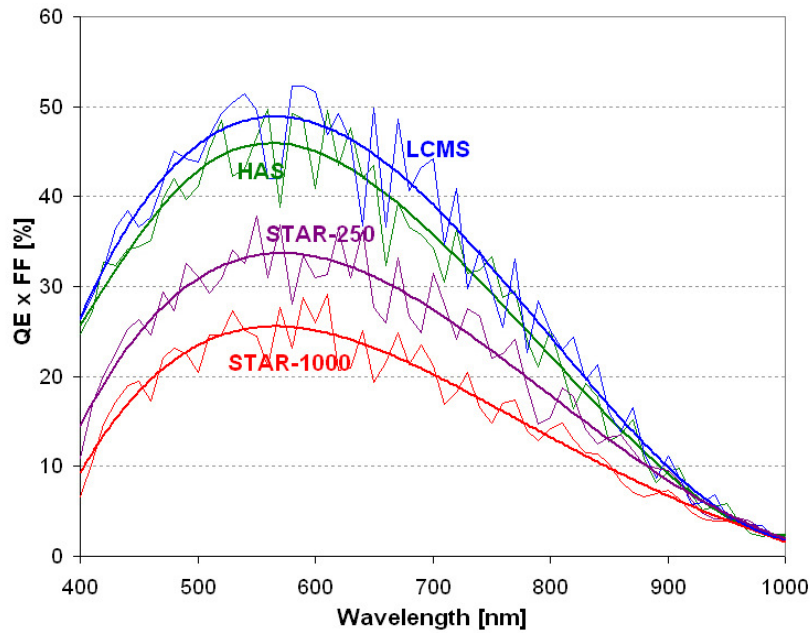*Figure 22.   Measured quantum efficiency (including fill factor) of the STAR, HAS and LCMS sensors.*

4.1.4.3 Photo-response measurement

Figure 23 shows the response curve with a fit to the linear response curve with the same conversion gain (solid black line). The dashed lines indicate linear response curves with –5% and +5% conversion gain.

The conversion gain is approximately 14.7 µV per electron and the full well charge is about 100 Ke. The linear full well charge (less than 5% deviation) is slightly larger than 80 Ke. In case a higher full well charge is needed, the sensor should be operated in 'hard reset' mode. This requires, however, a separate (higher) reset power supply voltage. Image lag, non-linearity near zero and dependency on the integration time (possibly all resulting from soft reset operation) has not yet been characterized (outside the scope of the contract).
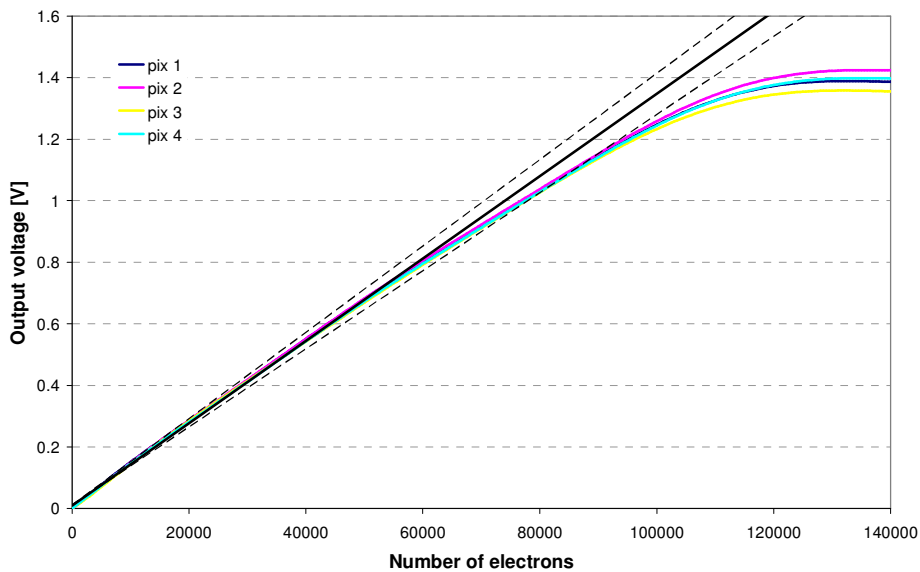

Figure 23.   Unity gain response curves of 4 pixels of one device.

4.1.4.4 Noise measurements

4.1.4.4.1   Fixed pattern noise (FPN)

FPN calculations were performed on images taken with short integration time (428 μs) in darkness. The FPN is calculated as the standard deviation of the residual offset after averaging 10 images. The measurements have been performed for different operation modes (normal double sampling mode (DS) and non-destructive readout (NDR)) and use of an external ADC or on-chip ADC. In each measurement, the different contributions in the FPN were calculated, i.e. global and local values (on 10x10 pixel windows), row, column and pixel contributions. The measurements were performed in the frequency range of 2.5 to 10 Mpixels/s.

Table 4.   Summary of FPN measurement with external ADC.

Requirement HAS sensor	Test result HAS sensor	Specification STAR-1000 sensor
45 electrons (local 10 x 10 pixels) < 15 with NDR (global)	45 electrons (local) 55 electrons (global) < 15 with NDR (global)	125 electrons (local) 365 electrons (global)

The FPN has also been measured during the total dose campaign (see further). We observe an increase in FPN at lower irradiation doses with afterwards a decrease of the FPN at higher total doses back to the initial level. Obviously, FPN reaches a maximum value near 20 krad(Si) and decreases afterwards. This can probably be attributed to the image lag behavior that is related to the soft reset operation that was used in these measurements.
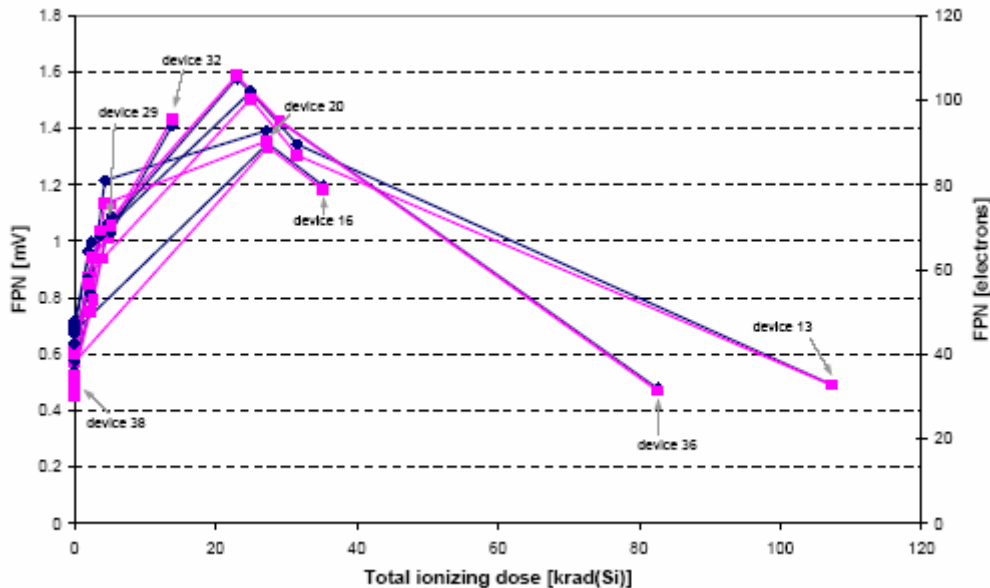

Figure 24.   FPN as function of total ionizing dose (Co-60 source).

4.1.4.4.2   Temporal noise

Dark noise calculations were performed on images taken with short integration time (428 μs) in darkness. The dark noise is calculated as the standard deviation of pixel values of an image obtained by subtracting two images and after division with sqrt(2). The measurements have been performed for different operation modes (normal double sampling mode (DS) and non-destructive readout (NDR)) and use of an external ADC or on-chip ADC. In each measurement, the different contributions in the dark noise were calculated, i.e. global and local values (on 10x10 pixel windows), row, column and pixel contributions. The measurements were performed in the frequency range of 2.5 to 10 Mpixels/s.

Table 5.   Summary of dark noise measurement.

Requirement HAS sensor	Test result HAS sensor	Specification STAR-1000 sensor
30 electrons	35 electrons (ext. ADC) 50 electrons (int. ADC)	> 60 electrons

The temporal noise has also been measured during the total dose campaign (see further). We observe a slight increase in noise. This can probably also be attributed to the image lag behavior that is related to the soft reset operation that was used in these measurements.
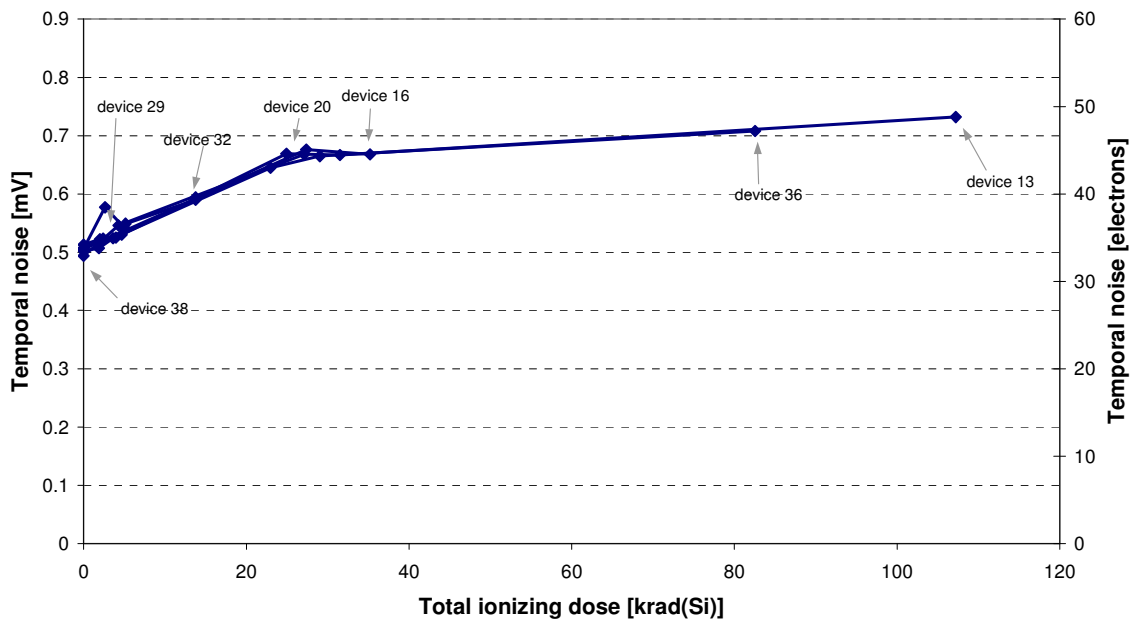
Figure 25.   Temporal noise as function of total ionizing dose (Co-60 source).

4.1.4.5   Dark current (DC) and dark current non-uniformity (DCNU)

The measurement results were calculated from an image that was obtained by subtracting an averaged image with short integration time (428 μs) from an averaged image with long integration time (7 s) (averaging both on 10 images). Figure 26 show the cumulative distributions of the dark current in e/s for the different devices and the average cumulative distribution (measurement at 25 ºC ambient temperature).

Figure 26.   Cumulative dark current distribution (in e/s) at 25 ºC ambient temperature.

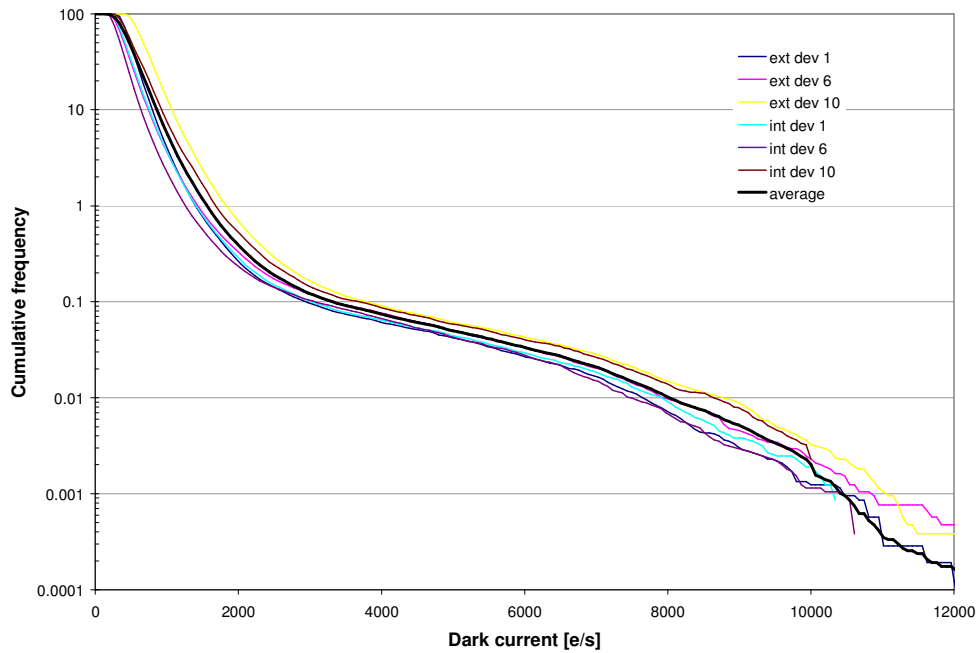The dark current has been measured as function of temperature (-20ºC to 60ºC) and total ionizing dose.

Following model could be consistent with what has been measured for *typical* values:

$$DC = DC_0\, 2^{\frac{T-T_0}{\Delta T_{DC,d1}}} + a_{DC}\, TID\, 2^{\frac{T-T_0}{\Delta T_{DC,d2}}}$$

$$DCNU = DCNU_0\, 2^{\frac{T-T_0}{\Delta T_{DCNU,d1}}} + a_{DCNU}\, TID\, 2^{\frac{T-T_0}{\Delta T_{DCNU,d2}}}$$

with   DC the dark current in e/s
         DC_0 the dark current at 30 °C and 0 krad = 300 e/s
         TID the total ionizing dose (in krad(Si))
         T the temperature (in °C)
         a_{DC} the slope of the curve at 30 °C = 325 e/s/krad(Si)
         $\Delta T_{DC,d1}$ = 5.8 °C and $\Delta T_{DC,d2}$ = 7.1 °C
         $DCNU_0$ the dark current non-uniformity at 30 °C and 0 krad = 230 e/s
         a_{DCNU} the slope of the curve at 30 °C = 33.6 e/s/krad(Si)
         $\Delta T_{DCNU,d1}$ = 9.5 °C and $\Delta T_{DCNU,d2}$ = 9.5 °C
         T_0 = 30 °C

4.1.4.6 Photo-response non-uniformity (PRNU)

The PRNU measurement is performed on a flat field illuminated image (600 nm, approximately at 50-70% full well) after subtraction of a dark image at the same integration time (to exclude influences of FPN and dark current non-uniformity). Both images are calculated first as an average of 10 images to minimize the influence of noise. Table 6 summarizes the result. Note that the local photo-response non-uniformity, measured as the average standard deviation calculated in each 5 x 5 pixel window, is only

marginally smaller than the global value calculated on a 100 x 100 pixel window. The measurement was not done on the whole pixel array because of the non-uniformity of the source. Values are believed to be within absolute accuracy of 0.1-0.2%.

Table 6. Overview of the PRNU measurement.

	DS				NDR	
in %	external ADC		internal ADC		external ADC	
	global	local	global	local	global	local
device 1	0.727	0.677	0.629	0.572	0.836	0.733
device 6	0.663	0.643	0.543	0.524	0.868	0.733
device 10	0.696	0.625	0.602	0.528	0.852	0.717

We could not observe any significant impact of the total dose irradiation on the photo-response non-uniformity.

4.1.4.7   MTF – pixel cross talk

Care has also been taken in the design phase to improve the pixel optical cross talk compared to that in the STAR-1000 and to obtain a very symmetrical pixel profile in both directions. This is shown in Figure 27. For this measurement, while moving a knife-edge over a particular pixel, the output voltage of this pixel is monitored as a function of stepping distance of the shadow. The figure shows the first derivative of the obtained output voltage curves. Due to asymmetry in the metal interconnections op top of the pixel, the pixel profile of the STAR-1000 is highly asymmetric and charges are spread over a larger number of pixels. The large improvement over the STAR-1000 in the symmetry of the response and the relatively low percentage of signal diffused into the second neighbouring pixels (about 1.3%) will result into an increased star centroiding performance.
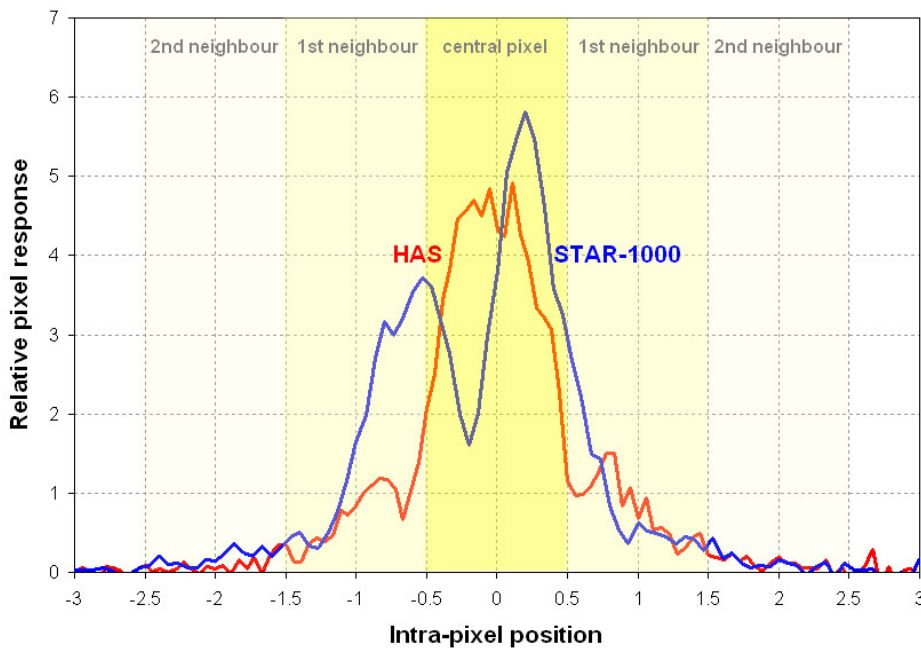

Figure 27.   Intra-pixel response of STAR-1000 and HAS obtained by knife-edge method.

4.1.4.8 Power consumption

The power consumption was measured at 5 Mpixels/s readout rate. The sensor core consumes about 65 mW.

Table 7. Summary of power consumption measurement.

Requirement HAS sensor	Test result HAS sensor	Specification STAR-1000 sensor
< 300 mW (including ADC) Goal: 150 mW	115 mW (including internal 12-bit ADC) (3.3 V power supply)	290 mW (including internal 10-bit ADC) (5 V power supply)

The average power consumption has been monitored throughout the measurement performed during the irradiation and afterwards. No measurable increase could be observed.
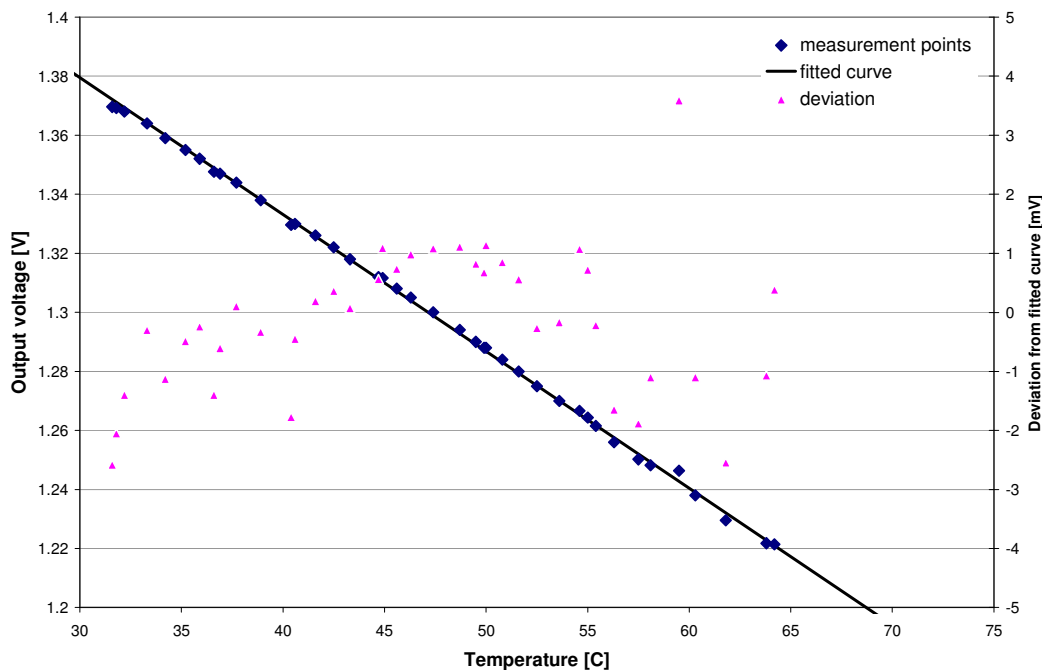
4.1.4.9 On-chip temperature sensor

Figure 28.   Temperature sensor voltage sensitivity. The solid line indicates a linear fit with 1.38 V as output voltage at 30 ºC and a slope of –4.64 mV/ºC.

4.1.4.10 Total dose radiation test

At ESTEC we have irradiated 6 devices using the Co-60 source. 1 device has been used as reference during the measurements and was also measured after each step (device 38). The total doses received by the different irradiated sensors ranged from a few krad(Si) to 107 krad(Si). The dose rate (about 1.5 krad(Si)/h) and time step were determined ad hoc at the facility and were depending on availability of the source and people. After a certain step (different for the different devices), the irradiation of a particular sensor was stopped, but still re-measured in following steps to study possible annealing effects.

After the irradiation, the following tests were performed at Estec:

- FPN and noise calculation: as result of the images taken during the irradiation campaign,
- Dark current and DCNU: as result of the images taken during the irradiation campaign,
- Dark current temperature dependence (only for device 13 and reference device 38)
- Response measurement (afterwards at Cypress facilities)
- Spectral response (afterwards at Cypress facilities)
- PRNU (afterwards at Cypress facilities)
- Power consumption

The results of these tests were summarized in previous paragraphs.

4.1.5 Conclusion of HAS development

Table 8 summarizes the most important specifications measured on the HAS sensor with comparison to those obtained on the STAR-1000. Although the sensors have a very similar architecture, only the HAS sensor allows for NDR, and therefore, easier simultaneous tracking of several windows combined with (off-chip) CDS.

Table 8. Overview of HAS sensor specifications with comparison to STAR-1000.

Parameter	Specification HAS sensor	Specification STAR-1000 sensor
Detector technology	CMOS Active Pixel Sensor	CMOS Active Pixel Sensor
Pixel structure	3-transistor active pixel Radiation-tolerant pixel design.	3-transistor active pixel Radiation-tolerant pixel design.
Photodiode	High fill factor photodiode, using n-well technique	High fill factor photodiode, using n-well technique
Technology	0.35 µm CMOS	0.5 µm CMOS
Sensitive area format	1024 x 1024 pixels	1024 x 1024 pixels
Pixel size	18 x 18 µm^2	15 x 15 µm^2
Pixel output rate	5 MHz (nominal) Speed can be exchanged for power consumption	5 MHz (nominal) Speed can be exchanged for power consumption
Windowing	X- and Y-addressing random programmable	X- and Y-addressing random programmable
Electronic shutter	Electronic rolling shutter. Integration time is variable in time steps equal to the row readout time. Possibility to have non-destructive readout (NDR).	Electronic rolling shutter. Integration time is variable in time steps equal to the row readout time.
Output range	1.3 V	1.1 V
Linear range	82000 electrons (linearity up to ± 5%)	70000 electrons (linearity up to ± 5%)
Charge to voltage conversion gain	14.8 µV/e	11.5 µV/e
QE x FF	40 % (average quantum efficiency for the wavelength range of 400 to 720 nm)	22 % (average quantum efficiency for the wavelength range of 400 to 720 nm)
Temporal noise	35 electrons (ext ADC) 50 electrons (int ADC)	60 electrons
FPN	45 electrons (local) 55 electrons (global)	125 electrons (local) 365 electrons (global)

Parameter	Specification HAS sensor	Specification STAR-1000 sensor
	< 15 with NDR (global)	
Average dark signal	115 electrons/s at 22 °C die temperature	785 electrons/s at 22 °C die temperature
DSNU	128 electrons/s at 22 °C die temperature	960 electrons/s at 22 °C die temperature
PRNU	0.7 % (global) 0.7 % (local)	3.3 % (global) 0.95 % (local)
Total Dose Radiation tolerance	> 100 krad(Si) average DS rise 150 e/s/krad(Si) at 22 °C average DSNU rise 18 e/s/krad(Si) at 22 °C	> 100 krad(Si) average DC rise 252 e/s/krad(Si) at 22 °C average DCNU rise 5 e/s/krad(Si) at 22 °C
Pixel tot pixel cross talk	10 % to neighbouring pixel	16 – 17.5 % to neighbouring pixel
Power consumption	115 mW (including internal 12-bit ADC) (3.3 V power supply)	290 mW (including internal 10-bit ADC) (5 V power supply)

The HAS sensor is capable of reading out 40 windows of 20 by 20 pixels (each) every 100 milliseconds, each having its own integration time, gain and offset. The offset and gain are settable by programming the corresponding on-chip registers. Despite the lower power supply voltage, the HAS sensor has a larger linear full well range and larger charge to voltage conversion gain, making the sensor less sensitive to system noise sources (quantization noise, electro-magnetic interference, power supply noise, etc). The table also clearly demonstrates the better performance in terms of noise and non-uniformity (both FPN and PRNU), quantum efficiency, pixel to pixel cross talk and power consumption. A high performance APS has been designed that is largely compliant to the initial specifications with an improvement in electro-optical performance over the existing devices.

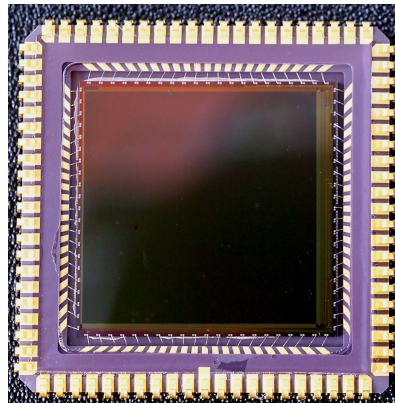A photograph of the HAS sensor is shown in Figure 29. The die measures about 21 x 21 mm^2.

Figure 29.   HAS die in 84-pin JLCC package.

The following list summarizes the requirements that were not yet demonstrated (with reference to par. 4.1.3) or outstanding future work:

- F4-F6: readout of different windows, different integrations times, different gain and offset: These requirements are not demonstrated simultaneously due to limitations in the test system. However, all operational functionality that is required for this specification has been tested and found in accordance to these specifications (functionality, upload of parameters, speed etc).
- E1, E3, E5, E8: Similarity with STAR1000.

- E2: operating range between –35 and +40 °C. No tests have been performed in range –35 to +25 degrees. No equipment available at Cypress facilities to perform these measurements at that time.
- E7: Outside of scope of the contract.
- Hard-to-soft operation mode

The following list summarizes the performance parameters that were found noncompliant to the specifications (with reference to par. 4.1.3):

- F1: 12-bit accuracy of the on-chip ADC: Due to small discontinuities at certain positions in the ADC transfer curve the ADC does not reach 12-bit accuracy (rather 10-bit effectively). To completely solve this problem, extensive simulations should be performed and/or alternative architectures must be investigated. At the same time, investments need to be done to be able to measure the ADCs accurately.
- P3: readout noise of less than 30 electrons. In DS mode, noise of 35 electrons is achieved using the external ADC and 50 electrons in case of the internal ADC. 30 electrons can possibly be achieved in a very well designed system in which system noise of all kind has been minimized. In our test system, we are obviously limited by system noise in NDR mode.
- P4: cross talk of less than 8% to neighboring pixel and invariant over life. Cross talk is estimated to be about 9.8% to neighboring pixel. Invariance over life is not yet demonstrated.
- P6: PRNU of less than 1.5% over the entire pixel array and less than 0.25% over any 5 x 5 sub-array of pixels. Global value is clearly achieved; local value is only slightly smaller than global value. This is a parameter that is limited by the used technology and cannot be improved by design as such.
- P7: DCNU of less than 250 e/pixel/second at EOL (1 sigma over all pixels). DCNU measured to be approximately 300 e/pixel/second at room temperature at BOL. DCNU typically increases in percentage of average DC when average DC decreases. Since average DC is very low, DCNU is almost 50 % of average DC. This is the current technological limit. Further reduction of the DC/DCNU can only be achieved by dedicated simulations on pixel profiles and technological efforts or by development of special pixel architectures.

4.2 LCMS

Originally ran as a parallel project to the High Accuracy star Sensor, the Low Cost low Mass star Sensor is a technology demonstrator for future highly-integrated sensor heads that enable star trackers to be built with smaller dimensions, lower mass, reduced system complexity, and lower power, while maintaining a minimal standard of performance (1σ noise of 4-7 arcseconds).

LCMS obtains this objective by using mixed-signal integration of circuits to directly reduce the number of system components and to reduce the requirements posed to the remaining components by off-loading some of their tasks:

- the sensor incorporates an ADC
- the sensor readout logic is moved from an FPGA to the sensor chip itself
- windowed readout intelligence is included on the sensor chip, taking the burden of window management away from the application processor
- pixel-rate data pre-processing is included, feeding presumed stars to the application processor as opposed to raw image data
- the use of accepted and wide-spread interface standards for commands and data, avoiding system level glue logic.

At the same time the innate analogue-domain performance of the LCMS is targeted to be of sufficient level to preclude the use of sensor cooling as well as sensor-specific artefact compensation processing at the application processor, further simplifying the system.
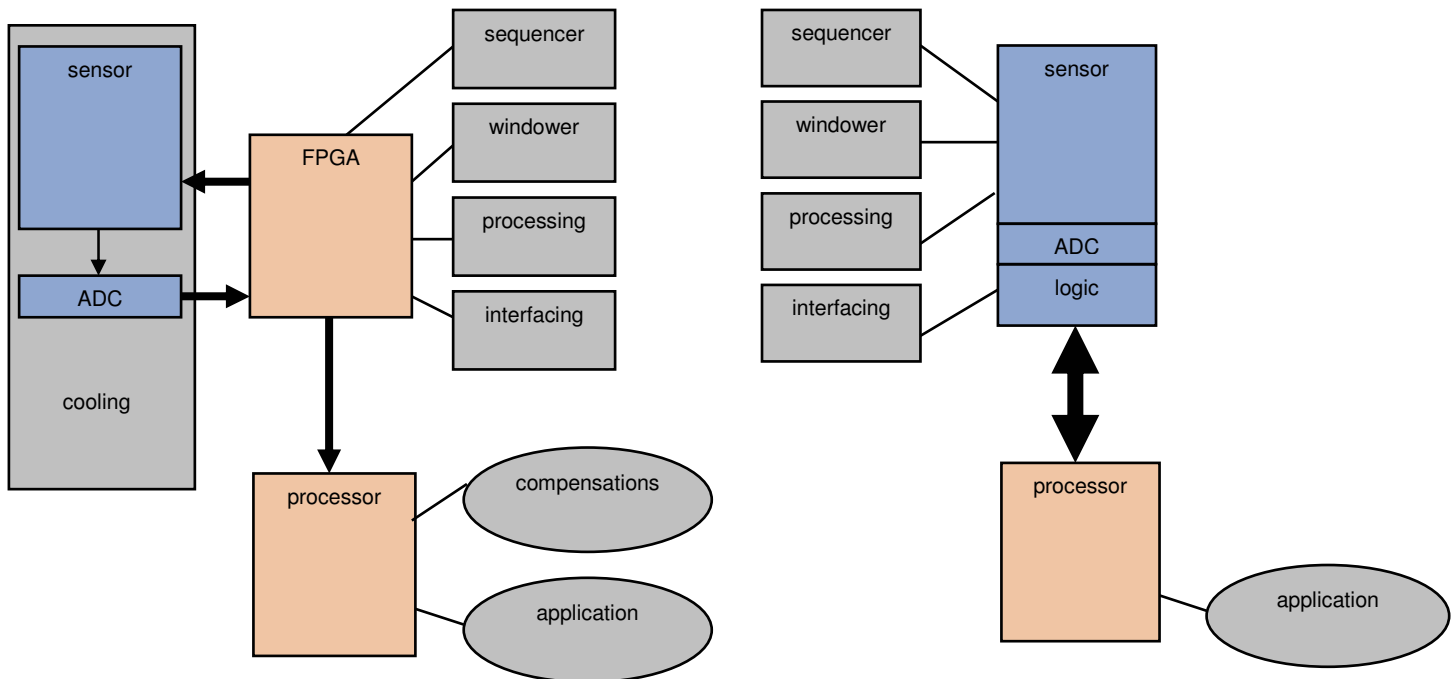

Figure 30. Typical system-level complexity: left for a HAS type of sensor, right for the LCMS sensor. Blue and orange denote system components. Grey denotes functionality attached to components.

4.2.1 Requirements

This section lists the requirements posed to the LCMS. These requirements originate both from ESTEC's initial analysis as well as a number of early design decisions based on the pre-existing HAS architecture and operational modes (e.g. Non Destructive Readout with digital Correlated Sampling, windowing, ...).

4.2.1.1 Functional requirements

Req. No.	Requirement
F1	The sensor shall provide a measure the amount of signal in each pixel as a digital count with 10 bit accuracy
F2	The Gain and Offset of the on chip ADC shall be dynamically settable.
F3	The sensor shall be capable of reading the entire pixel array at a frame rate of 5Hz (i.e. allowing a 200 ms integration time per pixel)
F4	The sensor shall be capable of reading out only pixels contained within selected windows.
F5	The sensor shall be capable of reading out 20 windows of 20*20 pixels at a rate of 10Hz (i.e. allowing a 100ms integration time per pixel)
F6	The sensor shall generate all the required timing signals and pulses to operate and control the light sensitive area via simple inputs from a user that will include an off-chip oscillator. To support this, the sensor will support 2 modes of operation – full frame readout and windowed readout. Full frame readout will allow the exposure and exposure start time to be specified by the user and shall readout the signal of every pixel in the array using a rolling shutter. Windowed readout will allow the exposure and start time to be specified by the user along with up to 20 non-overlapping windows that may be selected to be 10*10, 15*15 or 20*20 pixels.

F7	In full frame mode, the sensor shall be able to perform the following rudimentary pixel processing:
	  1.) Determination and output of the background signal level
	  2.) Thresholding of pixel values against a settable value that is added to the calculated background. (All those < are set to zero, all > are unaffected)

F8	The sensor functionality shall be modular in design such that it shall be easy to disable any non-required functionality either via bootstrap pins or user command. Disabling any functionality shall cause a corresponding reduction in power consumption.
F9	The sensor shall be capable of supporting adjustable pixel integration times with a set readout time. (e.g. 10Hz readout rate with pixel integration times of 5 to 100ms per pixel)
F10	The sensor shall be capable of writing the digital pixel data directly to an off chip memory.
F11	The on chip ADC shall be able to accept and digitise up to 4 externally provided analogue signals.
F12	The LCMS shall have a temperature monitor on chip.

4.2.1.2 Performance requirements

Req. No.	Requirement
P1	At BOL (i.e. zero radiation dose) the Dark Current shall be less than 2500 e/pixel/second at 25 degrees Celsius.

Req. No.	Requirement
P2	At EOL (i.e. full radiation dose) the Dark Current shall be less than 5000 e/pixel/second at 25 degrees Celsius.
P3	The sensor-reset noise (KTC Noise) shall be less than 75 electrons/pixel (1 sigma value over time and all pixels) at EOL.
P4	Cross Talk is defined as the % of the signal in one pixel that appears as a parasitic signal in a neighbouring pixel. The Cross Talk shall be less than 5% and shall be invariant over life.
P5	The Fixed Pattern Noise (FPN) shall be less than 75 electrons (1 sigma over the entire pixel array) at EOL.
P6	The Pixel Response Non Uniformity (PRNU) shall be less than 1.5% over the entire pixel array and less than 0.25% over any 5*5 sub-array of pixels.
P7	The Dark Current Non Uniformity (DCNU) shall be less than 3% at EOL (1 sigma over all pixels)
P8	The sensor shall have a response that is linear to within 0.5% over the range 0 – 80,000 electrons/pixel.
P9	The sensor shall have a sensitivity (defined as Fill factor * Quantum Efficiency) of greater than 40%.
P10	The sensor shall have an anti-blooming capability of at least 1000 times the full linear range.
P11	The spectral range of the sensor shall at least cover the wavelengths 0.4 to 0.9 microns.

4.2.1.3 Physical characteristics

Req. No.	Requirement
C1	The sensor shall be compatible with Pixel Array sizes of 384*384 to 640*640 pixels. The baseline array size shall be 512*512 pixels.
C2	The sensor active area shall be less than 17 * 17 mm, the maximum die size shall be less than 30*25 mm (TBC) and the maximum package size shall be less than 35*35 mm (TBC).
C3	The pixel dimensions shall be determined by the Contractor in order to comply with requirement C2 and the performance requirements but shall be greater than 23 microns along each side.
C3	The sensor power consumption shall be less than 400 mW at EOL and full speed operation.

4.2.1.4 Environmental requirements

Req. No.	Requirement
E1	The sensor End of Life (EOL) condition is defined as 15 years continuous operation in vacuum after being subjected to vibrations specified in Requirement E5 and the radiation dose specified in Requirement E6
E2	The sensor shall be compatible with an operating temperature range of –25 to + 50 degrees C
E3	The sensor shall be compatible with a non-operating temperature of –40 to + 100 degrees C
E4	The sensor shall be compatible with either a 3.3v or a 5v single power supply.
E5	The sensor shall be able to survive and operate nominally after being subjected to a random vibration for a duration of 2 minutes
E6	The sensor shall be able to survive and operate nominally after being subjected to a total ionising dose of 50Krads.
E7	The sensor shall be Single Event Latch up free under radiation with a Linear Energy Transfer
E8	The sensor shall be able to survive, without damage, a shock corresponding to 2000g for a 1000Hz half sine wave.

4.2.2   Design description

4.2.2.1   LCMS key specification

The LCMS is a 512 x 512 pixel single-chip star sensor head with on-chip 12-bit ADC, readout sequencer, soft-programmable window sequencer, digital-domain correlated double sampling (with on-chip memory for the storage of pixel black levels), star signal pre-processing (background determination and subtraction, thresholding). Command and data interfacing comprise of a number of configurable standard interfaces, including SpaceWire, RS-232, TTC-B-01, and FIFO inputs. Local telemetry can be done through four additional analogue inputs to the ADC and a temperature sensor.

Req. No.	Specification
optical format	512 x 512 pixels at 25 um pitch and with symmetrical optical profile
ADC	12 bit
signal amplifier	gain and offset control
pixel rate (max)	2.5 MHz
readout modes	Destructive Readout with Double Sampling (full frame and one large window) Non-Destructive Readout with on-chip digital-domain Correlated Double Sampling (up to 20 small windows)
windowed readout	up to 20 windows, sized 10x10, 15x15, or 20x20 pixels; per-window programmable start and end of exposure, gain, offset, position
window programming	freely-programmable, software-based
full frame rate	5 Hz
windowed frame rate	10 Hz
signal data processing	CDS; rolling background average with spike/star exclusion; background subtraction; pixel thresholding
command interface	SpaceWire (10 or 20MHz), asynchronous serial, synchronous serial (PacketWire, TTC-B_01, SPI)
data interface	SpaceWire (10 or 20MHz), parallel (FIFO-compatible)
auxiliary interfaces	4 additional analogue inputs to the ADC, temperature sensor
chip clock	20 MHz, external
IO levels	CMOS or LVDS (bond-option)
supply	single-supply 3.3V
package	JLCC-84

4.2.2.2   Technology choice

The processing technology of choice for the HAS was the XFab 0.35um CMOS process. At that time this was the process with the lowest dark current available to FillFactory, and the company used it to good effect for products for the high-end digital still camera market. Low dark current is of prime importance to noise-sensitive applications, including star tracking.

However, for practical reasons it was opted to manufacture the LCMS in the AMIs 0.35 um process, as opposed to XFab. At the start of the project FillFactory had no full in-house mixed signal design flow, and relied for the design back-end on subcontractor services (IMEC/Invomec). This subcontractor had
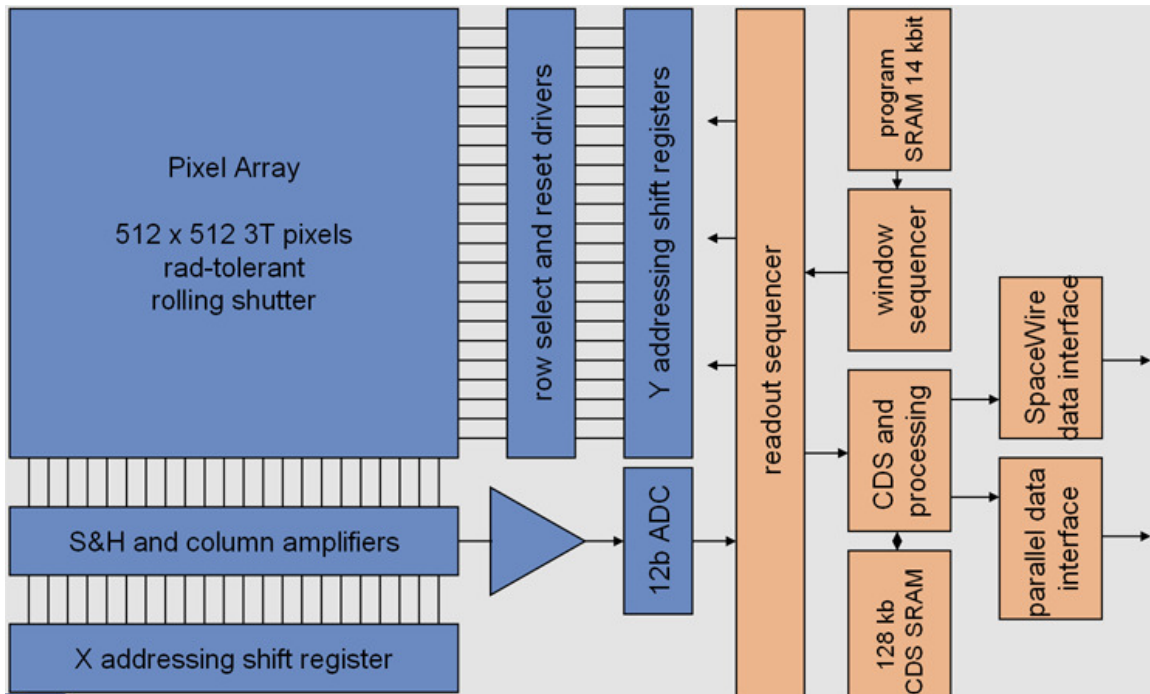
the full AMIs design suite installed, but not XFab. In addition, all IP required for making the LCMS was readily present for the AMIs process, while the situation with XFab was less clear.

For the sake of simplifying the design process and thus increasing the project's chance for success, it was decided to sacrifice some of the potential dark current performance.

4.2.2.3 LCMS chip architecture - block diagram

The blue sections in above block diagram reflect the HAS architecture. The orange blocks are the logic added to the analogue sensor core, comprising of readout sequencer, window managing sequencer and its program memory, CDS and pre processing block with its data memory, and the two main data output interfaces.
Not shown in the diagram are the command interfaces, central settings registers, and the telemetry inputs to the ADC.

All of these blocks will be discussed in the following sections.

4.2.2.4 Analogue sensor core and ADC

The LCMS's pixel array, analogue readout circuitry, and 12 bit ADC are a direct port of the HAS design from the XFab 0.35 process to the AMIs 0.35 process.
The only differences are:
- reduction of array size to 512 x 512 pixels (in line with the legacy STAR-250 sensor)
- growth of pixel size to 25 x 25
- layout rules with four metal layers (HAS: three); while this potentially has a negative impact on the optical performance, this is required to accommodate the mixed signal / logic IP on the chip.

The circuits and layout confirm to Cypress' rules for radiation-hard design.

The sensor core supports destructive readout (DS) with (uncorrelated) double sampling of signal and reset levels and analogue-domain Fixed Pattern Noise removal, as well as non-destructive readout (NDR) with correlated double sampling of reset and signal levels, and digital-domain (memory-based) removal of FPN and kTC noise.
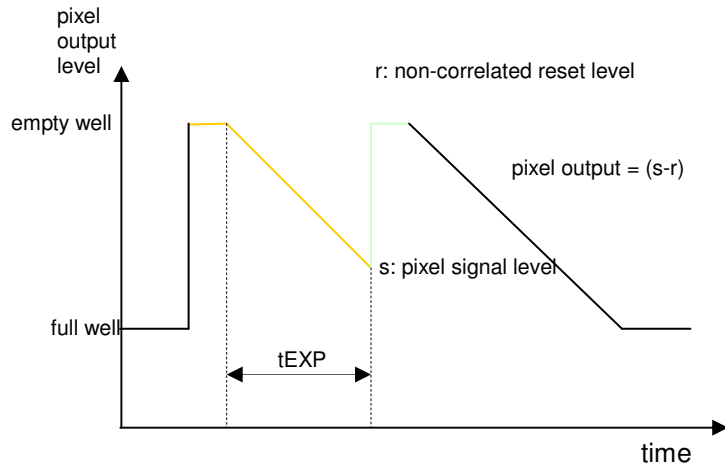
Figure 31. Destructive readout timeline; pixel output is the uncorrelated but near-instantaneously read difference of signal level ('s') and reset level ('r'), suppressing FPN but not kTC noise.
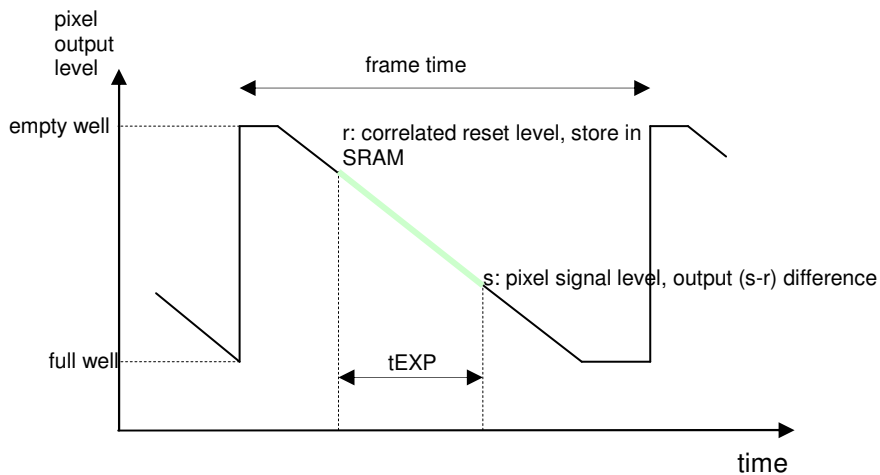

Figure 32. Non-destructive readout timeline: pixel output happens in two phases. First the reset level ('r') is output and stored externally in memory. After the exposure time the pixel is addressed again and its signal level ('s') is read and output. The correlated difference of s and r is the pixel signal value devoid of FPN and kTC noise.

For further details of the sensor core and ADC design the reader is referred to the relevant sections in the HAS Development Report (section 4.1).

4.2.2.5 Readout Sequencer

The Readout Sequencer is the single level of logic interfacing with the analogue sensor core and the ADC. The sequencer is responsible for controlling aspects of the analogue circuit, including its biasing householding and the actual image acquisition sequences.

The sequencer implements the two major modes of image capture: Destructive Readout (DR) on a full frame (or a windowed-down version thereof) and Non-Destructive Readout (NDR) on a single small window.

The former employs Fixed Pattern Noise correction in the analogue domain, yielding FPN-free pixel data at the output of the sequencer. The latter reads every pixel twice, first its post-reset black level ('r'), and after the exposure or integration time once more its signal ('s') level. Both levels are passed on downstream for CDS processing.

When scanning full-frame images in DR mode the sequencer operates autonomously, driving its data down the data path. In windowed NDR mode is the sequencer slaved to the Window Sequencer.

4.2.2.6 Window Sequencer

The Window Sequencer is responsible for the dynamic management of up to 20 windows in NDR/CDS mode. Each of these windows has its individual position, reset time, black-read time ('r'), signal read time ('s'), exposure time, amplifier gain, and amplifier offset.

The Window Sequencer repetitively executes a 'program' or timeline stored in on-chip SRAM memory. This memory contains 1024 locations, each holding a command requesting a specific action to a specific window. The whole memory is scanned every 100 ms, and each command encountered during this can is executed on the pixel array and readout sequencer. The granularity of timesteps, and thus of the commands, is approximately 100 ms / 1024 = 100 us.

The following commands are supported:
- RR: reset the whole pixel array
- R#: reset the window with number #
- r#: read the black/reset levels of the pixels in window # (and store them in the CDS memory)
- s#: read the signal levels of the pixels in window # (and process them for output)
- NOP: do nothing

The timeline programming method offers a very high flexibility in window management to the end-user, although the line-based nature of the LCMS's analogue pixel array poses some constraints:
- hard-resetting a window also resets any windows that share one or more lines with it; this can be avoided by starting every frame with a fast reset of all lines of the array, after which the windows are only ever read for black levels and signal levels (a non-destructive operation).
- every window accrues more or less dark current in the time that elapses between its reset ('R') and the readout of its black levels ('r').
- the user must be careful with updating the program or timeline memory while the system is operating in tracking/NDR/CDS mode lest program inconsistencies arise.

The program memory is 14 kbits large, organised as 1024 words of 14 bits. Each word has 4 bits for EDAC, allowing the detection and correction of one faulty bit per word. As the program stored in the memory is expected to be used for a relatively long time, each read access to the memory is accompanied with error correction and a write back of the data word. This hardens the SRAM long-term against SEUs.

The lower 40 locations in the program memory are not accessible for user commands. They are used for storing the X and Y start coordinates of the 20 windows. This was done to reduce the logic area and make the memory usage more efficient.

4.2.2.7 CDS and data Processing

In CDS/windowed mode pixel reset levels are retrieved from the sequencer and temporarily stored in an on-chip SRAM. After exposure pixel signal values are obtained from the array by the sequencer, and their corresponding reset levels are read back from the CDS memory. Each pixel reset level then is subtracted from its corresponding signal level, and the difference is output as a clean, FPN-free pixel value. On-chip CDS can be turned off, in which case both reset and signal levels are output to the user for further processing.

The CDS memory is sized 20 windows x (20 x 20) pixels x 16 bit = 128 kbits. Each 16 bit word holds a 12 bit pixel black value and 4 EDAC bits. The EDAC allow for the detection and correction of one faulty bit in the 11 upper bits of the pixel data payload. The data MSB is not protected. As black levels stored for CDS are single-use data no further protection against SEUs is present.
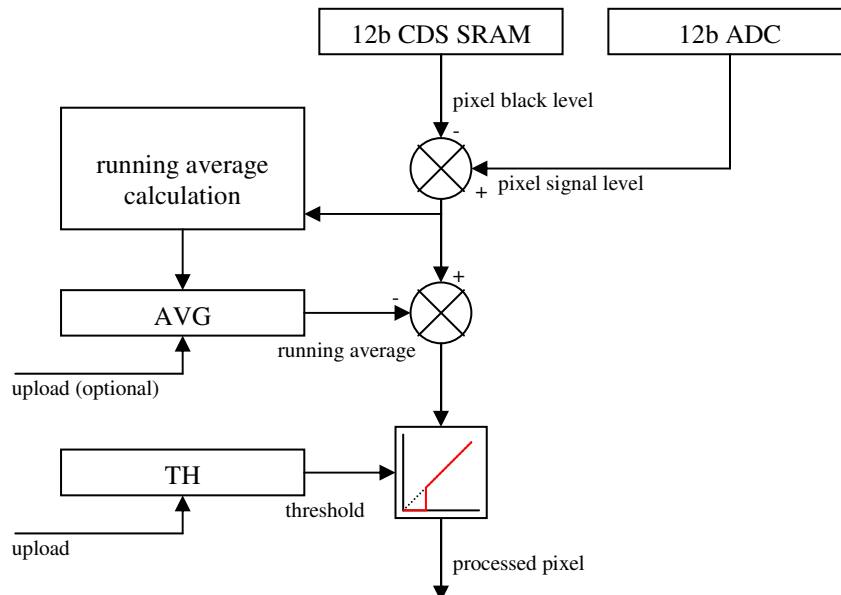

Figure 33.   NDR-mode pixel signal digital-domain processing flow.

The output of the CDS (in NDR/windowed mode) or of the sequencer (in DR/full frame mode) is subject to further processing (all of which can be bypassed):
- background determination with optional spike exclusion
- background subtraction
- pixel thresholding

Adaptive background determination:

The background intensity level around each output pixel is estimated, as a rolling average of 8 pixels along the line (X-direction). Pixels can optionally be excluded from this average when they exceed a user-programmable threshold. This avoids pixels that might belong to star spots being included in the background estimate.

The present background level estimate can be sent to the user at the end of each line (full frame mode) or at the end of each window (windowed mode).

Background subtraction:

Each pixel value can have the local background estimation value subtracted from it. This results in the effective removal of stray light from the source image, rendering the background homogeneously near-black.

Pixel thresholding:

Pixel values are compared to a user-programmed threshold value. Pixels not exceeding this threshold are set to zero value. The result is an output image (full frame or window) consisting of a hard-black background and a limited number of pixels that are presumed to belong to stars.

4.2.2.8 Data, Command, and Configuration Interfaces

Data interfaces:

The LCMS offers two types of data output interface: SpaceWire and Synchronous Parallel.

The SpaceWire interface is an implementation of an Astrium-sourced soft IP core (with a number of simplifying modifications). The interface is fully SpaceWire-compliant but is restricted to point-to-point use, the LCMS strictly being a slave device, and operation at 10Mbps or 20Mbps, i.e. considerably lower than the SpaceWire standard's 400Mbps maximum. The LCMS's SpaceWire link can sustain full frame readout at 5 frames per second, using data packing techniques to fold 12 bit pixel data into SpaceWire's 8 bit transport units.

The Synchronous Parallel data interface is a simple clock-synchronous parallel output bus, compatible with typical FIFO components, and easy to interface to FPGA or ASIC-based master systems. The bus sustains a maximum data rate of 2.5 MHz, equivalent to 9 full frames per second.

Command interfaces:

Commands enter the LCMS through three interface systems: SpaceWire, Universal Serial, and Parallel.

The command SpaceWire link is part of the whole SpaceWire IO system discussed in the previous paragraph.
The Universal Serial Interface can be configured for compatibility with the following standards:
- RS-232/485-like asynchronous
- SPI
- PacketWire
- TTC-B-01 8 bit and 16 bit

The parallel command interface uses the parallel data output bus reversed in direction. It is intended more for debug purposes than as a regular command input.

Configuration interface:

The device has a number of pins that are to be strapped to power or ground. These straps configure, statically, a number of LCMS options, including data and command interface selection and standard.

Devices are made in two versions (same die, different bonding):

LCMS-L supports only SpaceWire interfacing, employing full LVDS IO levels.
LCMS-C supports all interface types, employing standard CMOS IO levels.

4.2.2.9 LCMS physical and IP list

Figure 34.   LCMS die layout with main blocks indicated.

die statistics		units
X dimension	15.5	mm
Y dimension	16.2	mm
die area	251	sq.mm
logic cells	60	eq. kilogates
	15	sq.mm
program RAM	1.4	sq.mm
CDS RAM	9	sq.mm

The LCMS layout generation was subcontracted to Invomec, in close collaboration with FillFactory staff.

The external IP used comprises of:
- SpaceWire: soft (VHDL) core developed by Astrium (ESTEC contract 13345#3)
- SRAM: AMIs SPS2 (both)
- logic core cells: a subset of AMIs MTC45000 screened for low leakage
- IO cells: AMIs MTC45100 and MTC45105 (LVDS)

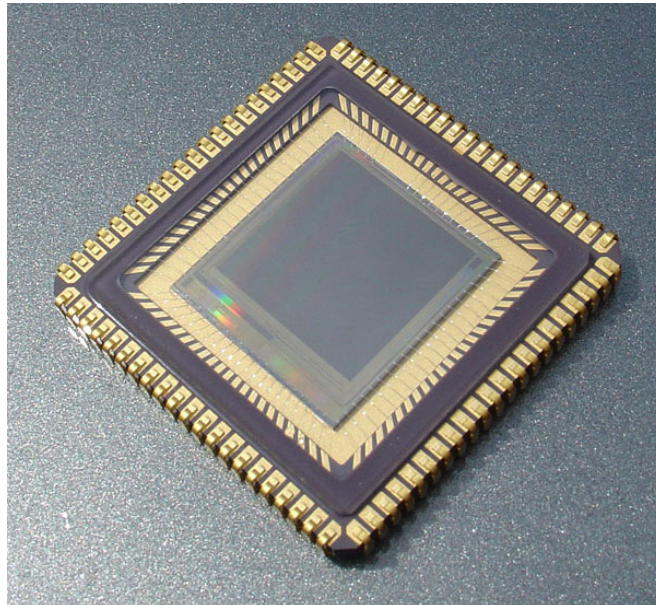The package is a ceramic JLCC84, identical to the STAR1000, STAR250, and HAS.

Figure 35.   LCMS in JLCC84 package.

4.2.3 Test plan

The following tests were executed on the LCMS:
- Functionality
- Electro-optical characterization
  - Spectral response
  - Photo response
  - PRNU & FPN
  - DC and DCNU
  - Noise
  - MTF and pixel profile
- Power consumption
- Total dose radiation (partial)

4.2.4 Test results

4.2.4.1 Functionality

The device was operational, in DR/DS as well as NDR/CDS modes, with serial/parallel interfaces and SpaceWire, including the LVDS option. A couple of very minor bugs were detected in the logic, all with easy work-arounds (described in the Datasheet).
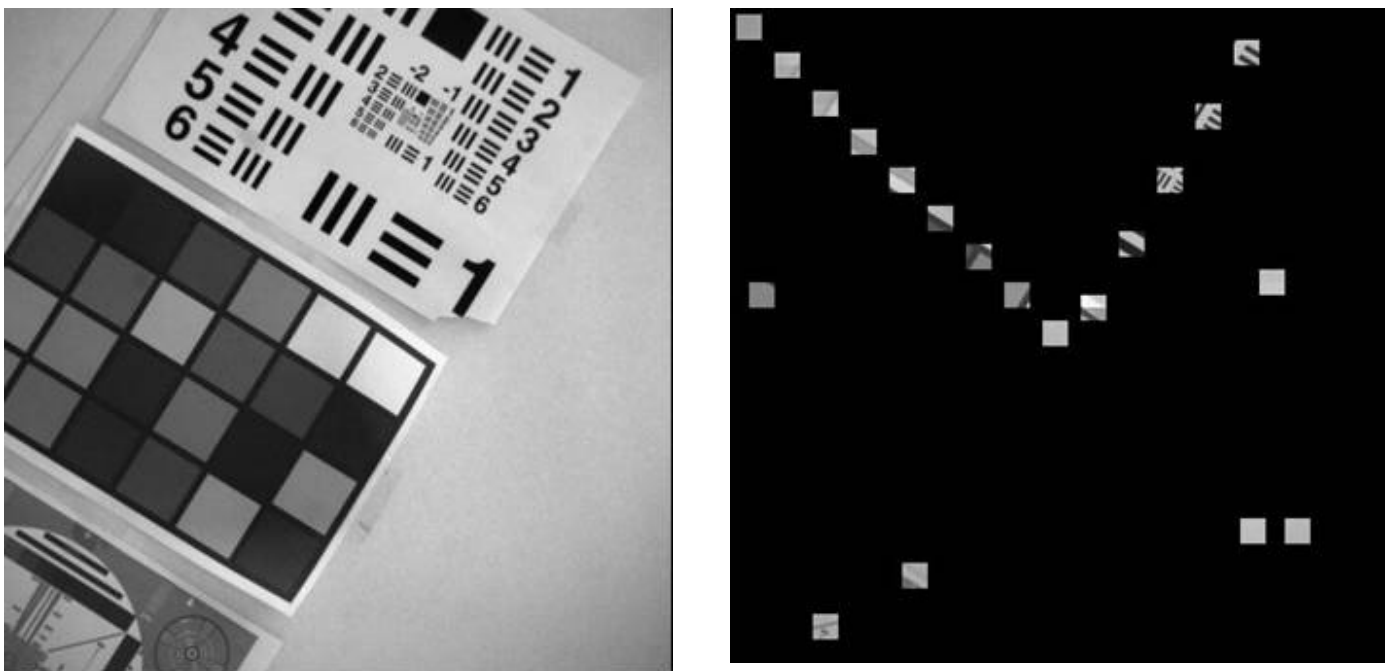

Figure 36.   Captured LCMS images. Left: destructive readout, double sampling. Right: non-destructive readout, correlated double sampling, 20 simultaneous windows.
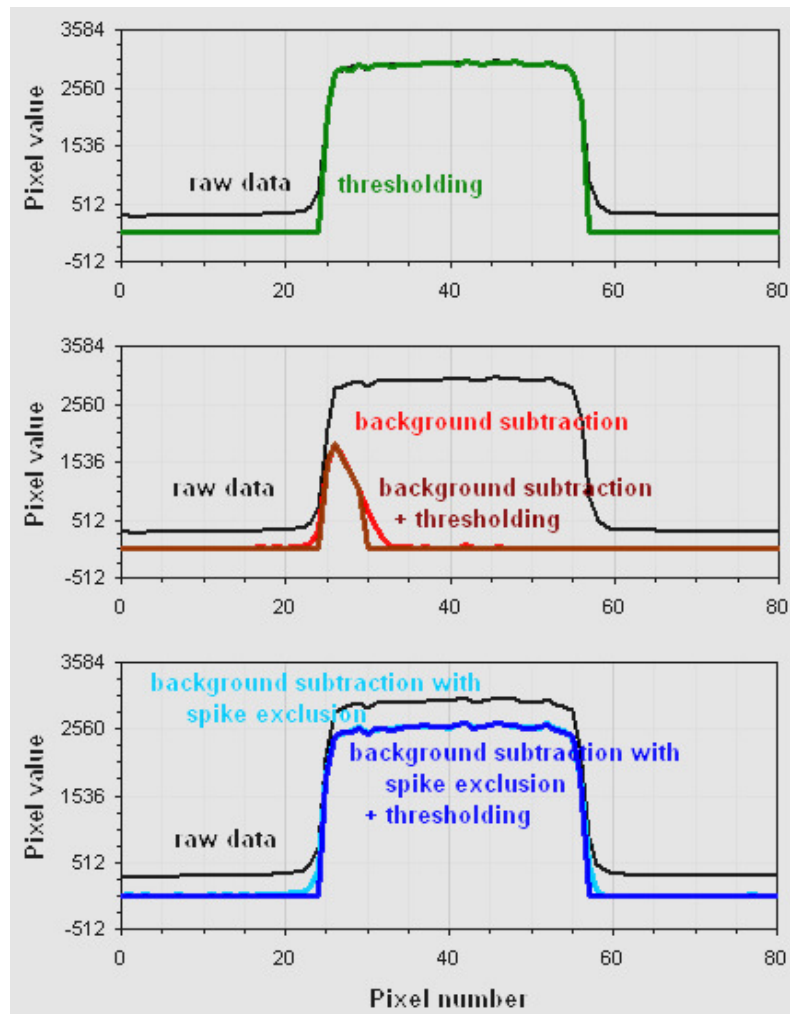
Figure 37.   Demonstration of pixel signal pre-processing.

Pixel pre-processing was demonstrated. Above figure shows the results of projecting a 30-pixel wide bright bar on the focal plane array, with increasingly more processing enabled. The upper figure demonstrates thresholding, where the background signal is effectively removed (note that in real-life this would require advance knowledge of the background level, to set the threshold value). The middle figure shows adaptive rolling-average background estimation and subtraction. Observe how at the rising edge of the pixel signal (left edge of the bright bar) the stored average lags behind the actual pixel signal, giving rise to a transient in the output, followed by the effective suppression of the bar signal. The lower graph demonstrates bright pixel exclusion from the average calculation, allowing the bright bar to pass through the processing chain undamaged.

These trials were fairly informal, using standard optical equipment available at Cypress. No effort was made to demonstrate the processing capabilities on real star data.

4.2.4.2 Performance and Environmental Summary

parameter	LCMS requirement	LCMS char result	Units	Remarks
Dark Current, BOL, 25C	2500	1000	e-/s	
Dark Current, EOL, 25C	5000	1000	e-/s	after 21.5 krad
Dark Current Non-Uniformity, 1sigma, EOL	5	100	%	
Read Noise, EOL, 1sigma	75	60	e-	after 21.5 krad
Pixel Crosstalk	8	10	%	
FPN, DR/DS, EOL, local	75	85	e-	after 21.5 krad
FPN, NDR/CDS, EOL, global	25	19	e-	after 21.5 krad
PRNU, global	1.5	1.4	%	
PRNU, local	0.25	1.0	%	
Linear Region, 5%	80000	30000	e-	monotonic
Linear Region, 15%		75000	e-	
Fill Factor x Quantum Eff.	40	40	%	
Power, full speed, EOL	400	164	mW	CMOS mode
		226	mW	LVDS mode
Total Dose Immunity	50	(21.5)	krad	test limit, device limit not known

Above table summarizes the characterisation results. Green rows contain parameters where the requirements were fully or almost met. Orange rows have parameters where the requirements were not met.

The excessive Dark Current Non-Uniformity is mostly a process property: porting the design to e.g. XFab 0.35 um would bring an improvement (see HAS results). Note that, here too, the absolute level of Dark Current is significantly lower than required.

Pixel transfer linearity is poor, but the transfer curve is monotonic, exhibiting a slight signal 'compressing' nature.
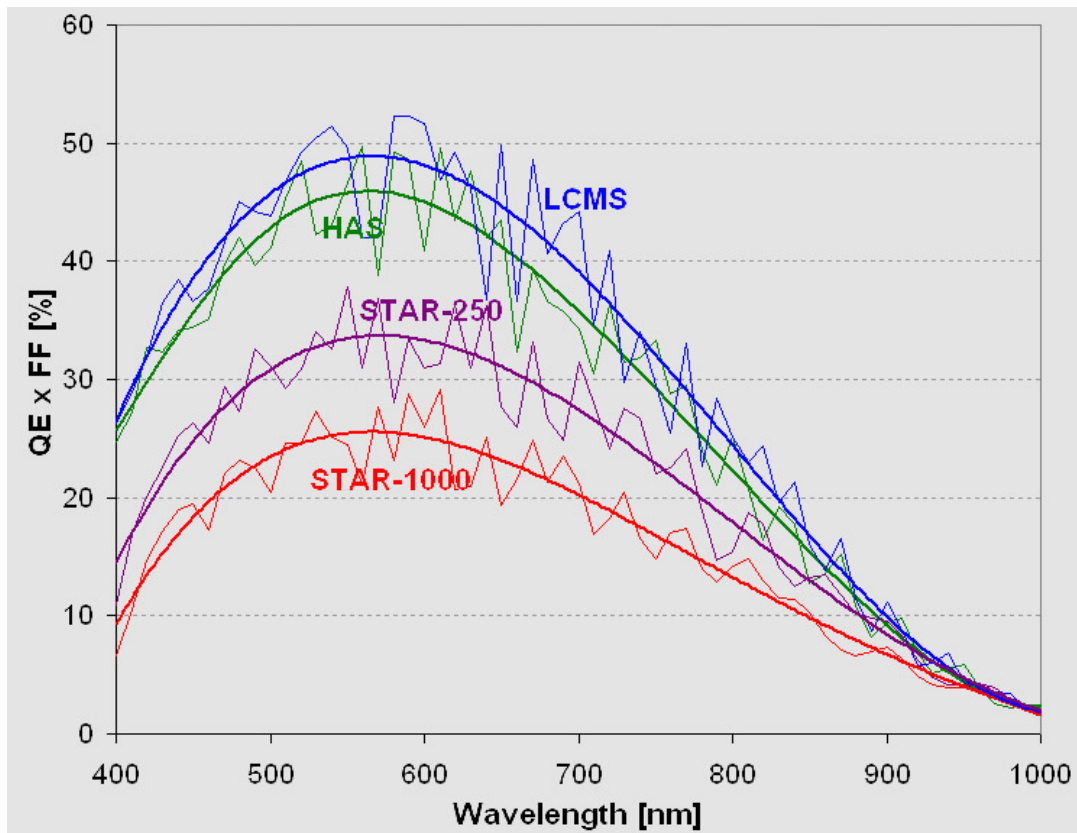
Figure 38.   LCMS product of Quantum Efficiency and Fill Factor, compared to HAS and STAR-250. Note that the STAR-250 has the same pixel size as LCMS!
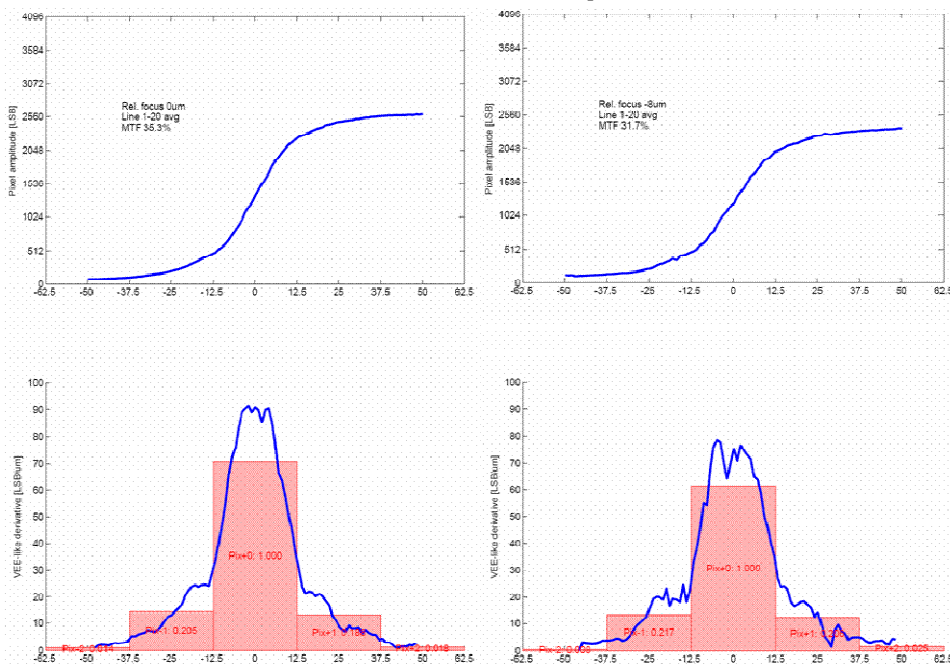

Figure 39.   LCMS optical pixel profile. MTF is 35% in the X-direction, 32% in Y.
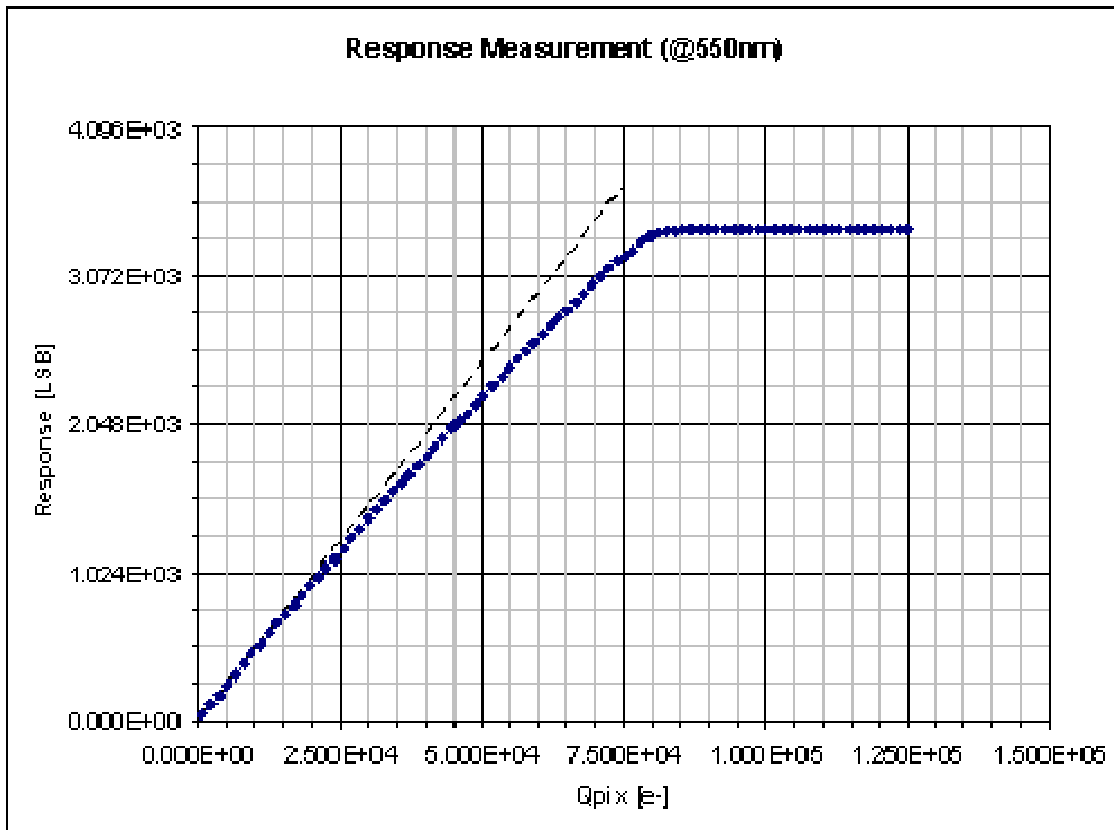
Figure 40. LCMS pixel transfer curve: pixel-site electronics to ADC codes. 5% linearity is 30000 electrons, but the curve is monotonic.

4.2.5   Conclusion

A demonstrator sensor chip for a compact star tracker head has been developed, using mixed-signal techniques to co-integrate the pixel array, readout electronics, ADC, readout logic, pixel data pre-processing logic, and advanced interfacing, including SpaceWire. The device employs on-chip memories for window timeline programming and for digital-domain correlated double sampling. The rad-hard analogue circuitry is closely based on the High Accuracy Star sensor design, while the on-chip logic uses commercial libraries combined with design techniques that afford a certain radiation tolerance.

Manufactured in the AMIs 0.35 um CMOS process, the LCMS proved to be fully functional. A limited characterisation program showed that it meets or approaches its performance requirements. The parameters where it failed its requirements are:
- FPN (marginally)
- local DCNU (meeting global DCNU)
- pixel response linearity

Additional test work is needed to characterise the device fully, including:
- total dose (beyond 21 krad)
- SEU and LU
- temperature
- vibration and shock

Notwithstanding the incomplete characterisation status we regard this development as a success.

5 General conclusion

During the evaluation project, a lot of knowledge was built up regarding evaluation of image sensors:

- Since a test house has not the same knowledge about image sensors, it is better to manage all the tests within Cypress and send out devices for individual tests. This requires more logistics but eases data evaluation and communication
- Some tests are not adequate for image sensors in general or for an 84pins JLCC device in particular. Especially on the mechanical tests additional work is to be done after the project.
- Some assembly configuration issues (e.g. N2 filling, other epoxy, …) have been implemented at the start of the project without detailed experiments. This is to be avoided.

The development of HAS and LCMS are successful. However for HAS a better on-chip ADC would be preferable. For flight missions a detailed evaluation program needs to be done. The lessons learned in the evaluation of STAR250 and STAR1000 will be used in this evaluation.